CHAPTER 5

Land-–-Seabed morphology and oceanographic processes in the Western Indian Ocean

Issufo Halo[1,2,3]

[1]*Conservation and Marine Sciences, Cape Peninsula University of Technology, Cape Town, 8000*
[2]*Centre for Sustainable Oceans Economy, Cape Peninsula University of Technology, Cape Town, 8000*
[3]*Nansen-Tutu Centre for Marine Environmental Research, University of Cape Town, Cape Town, 7701*

Commented [M1]: Must we have three addresses? Suggest author select one, max two, if possible.

Abstract

In this study a review of the relief of the earth's surface, which includes land-–seabed topography ~~on~~ of the Western Indian Ocean (WIO) is~~has been~~ presented based on a survey of published literature. The influence of such topographic features on physical oceanographic processes ~~was~~ is described on the basis of recent oceanographic data, which included: (1) twenty years of satellite altimetry observations of sea surface height variation and their derived geostrophic currents; (2) a mean dynamic topography computed from long-term model outputs, altimeter measurements and oceanographic in-situ data; (3) satellite observed windstress field and their derived windstress-curl; (4) and ocean-atmosphere density fluxes computed from hydrographic measurements. ~~Our~~ The analysis show that the long-term mean dynamic topography consistently portrayed well the main oceanographic features of the large-scale geostrophic surface circulation of the WIO region, with peak velocities of the mean flow of about 1.5 m s^{-1} in the Agulhas Current, at the southeastern rim of the Agulhas Bank. Inspections on windstress-curl revealed vigorous Ekman suction (pumping) events along the northern coast of Somali during the southeast monsoon winds, which suggests the occurrence of upwelling events near the coast, conversely downwelling slightly off-shore, especially from May to September. Similarly, in the northern tip of Madagascar a strong downwelling event occurs, conversely with an upwelling~~is~~ observed to the northwest of the Island. On the other hand, upwelling along the southern tip of Madagascar and along the southeast coast of South Africa are evident during the northeast m~~M~~onsoon period. Monthly climatological maps of sea level anomalies (SLA) over the annual cycle revealed a strong seasonality, with significant regional variabilities. Larger and predominantly zonally elongated features dominated in the northwest Indian Ocean, while a more circular geometric structures dominated in the southwest Indian Ocean. These appear to suggest an interplay of different mesoscale processes, namely Rossby waves and eddies. An automatic eddy tracking algorithm was used to identify and track in space and time mesoscale eddies from altimetry maps of absolute dynamic topography over a period of twenty-years. Statistical census o~~n~~ the eddy field revealed different spatial/temporal distribution patterns between the northwest and southwest Indian Ocean sectors, separated by a strong eddy desert region between 12°S and 3-°N. Many mesoscale structures in this latitude band had relatively short lifespan, lasting ~~lived~~ less than three months. Geometrical patterns of sea level anomalies in such a latitude band suggest their identity as baroclinic Rossby waves. Overall, more cyclonic than anticyclonic eddies were found, and all tracked structures exhibited a predominant westward and southwestward propagation, which were heavily impacted by the seabed morphology, continental land masses, islands and bathymetric ridges. These highlight the role that bottom topography plays in influencing oceanographic circulation processes ~~of the circulation~~. The eddy trajectories strongly suggest an effective inter-basin telecommunication which could potentially favor connectivity pathways of oceanic materials. The

Commented [M2]: Is this correct, latitude band?

eddies also play a noticeable role ien the distribution of surface chlorophyll, especially in coastal upwelling dominated areas. Comparison between monthly climatology maps of SLA and ocean-atmosphere density fluxes strongly suggested a weakening of the SLA in the greater Agulhas system during the periods of strong positive density fluxes, indicative of strong surface cooling events, especially between May and August.

Keywords:

Topography, seasonality, mMonsoons, ENSO, IOD, mMesoscale-eddies, wWindstress-curl, uUpwelling

Introduction

On a global scale, analysis of histogram of the Earth's solid surface (which account for land topography, and ocean bathymetry) by means of a hypsographic curve, shows that the continents are several hundred meters above the sea-level, while the oceans are about 4300 m below. A great deal of geological processes across several time and space scales are known to drive the land and seafloor morphology of the earth's surface (Parson and Evans, 2005). In some cases, these forcings, both in the vertical and horizontal directions, have ~~established~~ resulted in unique morphologies~~y~~, eg- upwarping and down-dropping along the fracture zone of the East Africa tectonic plate (Pepper and Everhart, 1963). Massive uplifting land topography on the reams of the ~~western Indian Ocean (~~WIO~~)~~ countries plays an important role in modulating various geologic processes (Oettli and Camberlin, 2005) and services across multi-disciplinary sciences (UMLP, 2016), eg historical migration of the hominids over the past ~~8~~ eight million years (Myr), agricultural practices (Sepulchre et al., 2006) as well as the evolution of the atmosphere, ocean and ecological systems across various trophic levels (Spencer et al., 2005). It has been hypothesized that the uplifting of the eastern Africa land topography has induced a significant abrupt re-structuring of atmospheric circulation with significant impact on moisture transports and precipitation (Sepulchre et al., 2006; Jung et al., 2016). Studies suggest that the eastern Africa topography has an influence on seasonal rainfall distribution (Oettli and Camberlin, 2005; Yang et al., 2015). The runoff becomes one of the most important physical mechanisms responsible for the export and deposition of land-based material into the sea, thus shaping the coastline and seafloor configuration (Moore et al., 2009; Partridge et al., 2010; Fenta et al., 2020).

On the other hand the seafloor morphology and bathymetric relief (eg islands, ridges, banks, abysses, canyons) in the WIO region (Fig. 1a) influence the hydrographic and dynamical behaviour of dominant oceanographic processes, such as the intensity of mean currents; filaments, fronts, eddy generation, eddy propagation, pathways and decay of vortex structures (eg meanders, rings and eddies); hotspot formation of internal waves; ocean-atmosphere flux exchanges, vertical mixing, mass/volume transports, and the development of upwelling/downwelling events, etc. (Matano et al., 1999; Ansorge and Lutjeharms, 2003; Parson and Evans, 2005; Spencer et al., 2005; Penven et al., 2006; Lutjeharms, 2006; Read and Pollard, 2017; Pollard and Read, 2017). Many of these processes, either isolated or combined, have a strong impact on the composition, state, and functioning of the regional ecosystems (Partridge et al., 2010; Barlow et al., 2014).

Therefore, in this chapter ~~we~~ the aim is to ~~at~~ present~~ing~~ a detailed and comprehensive description of the characteristics of the land and ocean bottom topography of the WIO (Fig. 1b-c), based on the best available scientific information of the region, assessed through published material. Among many, an important study to highlight in this chapter is the extensive work conducted and published ~~at~~ by an anonymous professor of the U~~u~~niversity of Minnesota Library (hereafter UMPL), Minneapolis, ~~(~~USA~~)~~, ~~by an anonymous professor who have requested conceal of his identity by the publisher. Thus forcing us to use~~ cited ~~here the acronym~~as UMLP (2016).

In addition to ~~our~~ the review, wherever ~~deemed necessary~~appropriate, the description is ~~we~~ complemented ~~our description~~ by analysing recent observed datasets freely available through the worldwide web, such as global earth bathymetric chart of the oceans (GEBCO, https://www.gebco.net/data_and_products/gridded_bathymetry_data/), global mean dynamic topography of the oceans (CNES-CLS09 MDT), satellite altimetry derived maps of absolute dynamic topography (MADT) and their derived fields of geostrophic currents (http: //marine.copernicus.eu/), satellite windstress fields derived from Scatterometer Climatology of Ocean Winds (SCOW, http: //numbat.coas.oregonstate.edu/scow/), and ocean-atmosphere surface density fluxes computed from long-term hydrographic thermal and haline properties derived from the world ocean atlas database (WOA, https://www.nodc.noaa.gov/OC5/woa18/woa18data.html/)~~ database~~. These allows us to

Commented [M3]: Numbered sections are not part of the layout design.

Formatted: Highlight

Commented [M4]: I don't think we need to explain the reason for the reference, if this is how the source material is usually cited.

capitalize on relevant oceanographic processes such as mesoscale variability, eddies, and hydrological properties, somehow linked to the prominent bathymetric configurations that have a significant impact on shaping the WIO's habitat systems, classified as "critical".

~~2.~~ Land Morphology

~~2.1.~~ *Continental mainland morphology*

Fig. 1b-c shows a three-dimensional view of the Earth's solid surface (land–ocean), derived from GEBCO dataset, mapped for the ~~Western Indian Ocean (~~WIO~~)~~, here defined as the region spanning from 10–80◦E and 50◦S–30◦N. For the purpose of detailed visualization of the topographic features we have presented Fig. 1 in two different three-dimensional perspectives (Fig. 1a, b). From south to north, the land topography starts first by depicting the South African continental morphology (Fig. 1a-b), known to have a higher surface elevation that covers more than 40 per cent of the total land surface area of about 1.22 million km^2, and the mean altitude is about 1200 m (Bond, 1979). The surface land encompasses three main regions: (i) marginal region with a width ranging between 80 and 240 km in the east, and between 60 and 80 km in the west; (ii) the interior plateau, which separates from the marginal regions by means of the Great Escarpment; and (iii) the Kalahari Basin (Kruger, 1983). The land upslopes from west to east towards the Drakensberg M~~m~~ountains, where the tallest mountain is the Injasuti Mountain with an altitude of about 3408 m, near the border with Lesotho (Moore et al., 2009; Partridge et al., 2010). From Drakensberg the terrain downslopes eastward towards the Indian Ocean (Fig. 1c) passing through the hills and narrow coastal plain in the valleys of KwaZulu~~the~~ Natal (Fig. 1a). The country's total coastline is about 2–798 km, and the climate is predominantly semi-arid and subtropical along the east coast, with an average precipitation of about 495 mm year^{-1} (Partridge et al., 2010).

Extending northward along the coast bordering the Indian Ocean, the political boundary separates South Africa from Mozambique (Fig. 1a). Mozambique has a surface area of nearly 800 000 km^2 (Cabral et al., 2017) and the stretched coastline is about 2~~,~~800 km long (Palalane et al., 2016). The terrain is characterized mostly by low coastal plains and in the central interior it is elevated (Fig. 1b-c). The plateau~~s~~ lies on the northwest of the country marked by a range of mountains on the western part. The climate is tropical to subtropical, and the average rainfall is about 1~~,~~032 mm year^{-1} (Partridge et al., 2010).

To the north of Mozambique lies the United Republic of Tanzania (URT) (Fig. 1a), with a surface area of about 945 090 km^2. Like in Mozambique, the terrain is also variable, characterized by coastal plains, plateaus in the centre, and highlands in the northern and southern parts of the country (Fig. 1b-c). The country hosts the highest mountain in Africa, the Kilimanjaro, which has an altitude of about 5~~-~~894.83 m high (UMLP, 2016., Fenta et al., 2020), and is located close to the border with Kenya. The climate varies, being of tropical nature in the coast and temperate in the highlands. The average rainfall is estimated in 1-071 mm year^{-1} (Westeberg and Christiansson, 1999; NationMaster, 2018).

To the north of Tanzania along the Indian Ocean lies Kenya (Fig. 1a), which encompasses a surface area of about 569,250 km^2, with a relatively shorter coastline of about 536 km (Westeberg and Christiansson, 1999; Fenta et al., 2020). The surface land is characterized by low plains that ascend to the central highlands (Fig. 1b-c), which are then bisected by the Great Rift Valley, while the plateaus lie to the western side. The country hosts the second highest mountain in Africa, the Mount Kenya, which has an altitude of about 5~~-~~199.28 m, and is located to the north of the Nairobi capital city, near the E~~e~~quator. The climate varies from tropical along the coast to arid in the centre interior. Both Kilimanjaro in Tanzania and Mount Kenyan ~~Mounts~~ are located to the east of the East Rift Valley and are characterized by inactive volcanoes and have permanent snowing regime at their summits~~tops~~ (UMLP, 2016). They are providers of freshwater to the low-land surrounding areas. Nevertheless, there are also some active

volcanoes in some relatively low range altitude mountains such as the Ol-Doinyo Lengai (Westeberg and Christiansson, 1999).

Somalia is located to the north of Kenya (Fig. 1a), occupying a surface area of about 637 650 km^2, and a coastline of about 3~~-~~025 km (Leslie, 1991), which is the longest along the eastern African continent. The land topography is mostly flat ~~to~~ with an undulating plateau rising to high elevations in the north. Leslie (1991) indicates that the central and southern parts of Somalia are mostly plain and plateau. This feature is contrasted with that in the north which is mountainous, whereby some peaks can reach more than 2000 m above ~~the~~ sea level (Fig. 1b-c). The climate is predominantly desert, with strong influence of the northeast and southwest monsoons, spanning from December to February and May to October, respectively. It is moderate in the north and hot in the south, typical of the southwest monsoon season. During the northeast monsoon the climate is torrid in the north and hot in the south. During the transitional phases of the monsoons the climate is characterized by irregular rainfall events with hot and humid periods. Past studies revealed that larger parts of the country receive less than 300 mm year^{-1}. The overall annual average of the rains is 2-330 mm year^{-1} (NationMaster, 2018).

~~2.2.~~ *Islands morphology*

To the east of the African mainland lie the several island states of the ~~Western Indian Ocean~~WIO (Fig. 1a). The island of Madagascar is the largest ~~one~~ (it being ~~is~~ the world's fourth-largest), and is located at about 415 km away from the African mainland (Fig. 1a). It is thought that the island broke away from the main continent more than 160 million years ago (Ma), thus developing its unique environmental characteristics. The island is about 1400 m above ~~the~~ sea level (Southall, https://www.britannica.com/place/Madagascar) and its surface area is about 587 040 km^2, and the coastline is about 4~~-~~828 km long. The land morphology is characterized by narrow coastal plain and high plateaus and mountains in the centre (UMLP, 2016). The summit of the Tsaratanana massif, known as the Maromokotro is about 2~~–~~876 m in altitude, and the tip of the Ankaratra massif, known as the Tsiafajavanova is about 2~~–~~643 m (Southall, https://www.britannica.com/place/Madagascar). The climate is tropical along the coast, temperate inland, and arid in the south. The average rainfall is about 1~~,~~513 mm year^{-1} (NationMaster, 2018). Tropical rain forests are located on the eastern edge on the windward side of the island, whereas the western side is characterized by rain shadow effect, receiving lower precipitation rates.

Commented [M5]: Is it acceptable to cite the Britannica Encyclopedia, and to do it like this? Who is Southall?

Madagascar is surrounded by several independent island states to the north, namely, Comoros, Seychelles and to the east by Reunion and Mauritius Islands (Fig. 1a). The Comoros is an archipelago located at the northern ~~gate~~ entrance of the Mozambique Channel, between Madagascar and northern Mozambique (Fig. 1a). The archipelago hosts four main islands, Grande Comore, Mohéli, Anjouan, and Mayotte (Fig. 2e). The distance between the first two islands is about 40 km, and between the last two is about 80 km (Goodman et al., 2010). Its surface area is about 2-230 km^2, and an extension of coastline of about 340 km ~~long~~. The islands are oceanic of volcanic origin (Harris and Rocha, 2009), varying from steep mountains to low hills in the interior. The climate is marine tropical with rainy seasons between the months of November and May (Harris and Rocha, 2009) and the average rainfall is about 900 mm year^{-1} (NationMaster, 2018). Mayotte Island in the archipelago is the closest to Madagascar by 300 km (Fig. 2e), and it has a surface area of about 37 km^2, and a coastline of 185.2 km. The terrain is bumping with deep ravines and ancient volcanic peaks. It is characterized by a tropical, marine, hot, humid rainy climate during the northeast monsoon (November ~~-~~ May), while cooler ~~-~~ dry season dominates during the southwest monsoon.

To the north of Madagascar lies the Seychelles ~~Islands~~ (Fig. 1a, Fig. 2h), occupying a surface area of about 460 km^2, and a coastline of about 491 km long. The largest~~y~~ are characterized by a granitic narrow coastal strip, being rocky and hilly. ~~It~~ Many of the smaller islands of the Seychelles ~~also encompasses~~are coral flats and elevated reefs. The climate is tropical marine. During the southeast monsoon the climate is humid and cool, from late May to September, while ~~. On the other hand,~~ it is warmer during the

northwest monsoon, between March and May. The average rainfall is about 2–330 mm year^{-1} (NationMaster, 2018).

To the east of Madagascar lies the volcanic Island of Reunion (Fig. 1a, Fig. 2e). The coastline has an extension of about 207 km long, and theits irrigated land covers about 120 km^2. The terrain is predominantly rugged and mountainous, with fertile low-lands along the coast. Maximum altitude is the mount Piton des Neiges with an elevation of about 3–069 m high. The climate is tropical but gets moderated with altitude. It is cool and dry between May and November, but hot and rainy between November and April.

Further east of Reunion Island lies the Mauritius Island (Fig. 1a, Fig. 2e). It covers a surface area of about 2–040 km^2, and a coastline length of about 177 km. It is characterized by small coastal plains and discontinuous mountains that encircle a central plateau. The climate is tropical, modified by the southeast trade winds. It has warm and dry winters between May and November, and hot, wet and humid during summer, which is extended between December and April (NationMaster, 2018). The smaller sister island of Rodrigues lies further to the east.

3. Seafloor Morphology

The morphology of the world's ocean sea-floor topography is divided in three oceanic provinces, namely, (i) continental margin, (ii) deep ocean-basins (abyssal plains), and (iii) mid-ocean ridges. While limited and scanty, scientific studies to-date conducted in the WIO region provide a great deal of details from which it is possible allow to infer that the seafloor topography of this region is unique (Fig. 1). Some of the peculiarities have been highlighted in several published material, and include: (i) it is composed by all types of tectonic plate boundaries of active and fossil composition, (ii) it encompasses some of the most deep-reaching fracture zones (Parson and Evans, 2005); (iii) it is dominated by an array of several mid-oceanic ridges (Fig. 1), which have nearly a meridional orientation (Defant, 1961; Tomczak and Godfrey, 1994); with (iv) some of the thickest sedimentary settlements of the world's ocean basins (Parson and Evans, 2005).

4. Continental Margins

The continental margin is the domain that stretches from the littoral up to the end of the continental rise (or beginning of the deep ocean basins). It comprises three important bathymetric features, namely, (i) continental shelf, (ii) continental slope and (iii) continental rise. The boundaries of the deep ocean basins in the WIO region are generally of non-volcanic origins, with passive rift geometries, floored extensively by moderate sediment cover. They are characterized by continental shelves of variable forms and dimensions (Parson and Evans, 2005). In the fFollowing sections are we presented an account of some of the most prominent features of the WIO continental shelves.

4.1. Continental Shelves, Banks and Bights

The continental shelf is an integral part of the continental margins, which extends from the littoral to locus where its profile depth steepens abruptly (shelf-break). The shelves are commonly characterized by gentle slopes, and the isobaths of 200 m contour is generally referred as their average extension. They encompass banks, bights, bigots, etc., and are generally floored by coastal rocks and sediments eroded from the inner-land environment. In the WIO region, adjacent to the African continent, one of the most prominent continental shelf is the Agulhas Bank, located directly to the south of South Africa (Fig. 2a). The second after this is the Sofala Bank, in central Mozambique (Fig. 2d). Apart from these, elsewhere the continental shelves of the WIO region are relatively narrow strips (Pepper and Everhart, 1963).

Commented [M6]: Please clarify ".. littoral to locus..". Something missing?

4.1.1. South African south and south-eastern continental shelves

The Agulhas Bank is a broad, near-triangular bathymetric protrusion of the continental shelf, lying at the southern tip of Africa (Fig. 2a). The Bank extents southward, from the coast to a maximum distance of about 300 km. It has an area of about 80 000 km^2 (Lutjeharms and Cooper, 1996), and is largely dominated by broad platforms of rocks believed to be from Palaeozoic age, mixed with sediments of Tertiary and more recent ages (Pepper and Everhart, 1963). The morphology of the Bank suggests that this feature may have been affected by tectonic forces that thrust inland from the sea to form narrow east-west folds of Cape Mountains (Pepper and Everhart, 1963). The topography of the Agulhas Bank can be divided in two distinct domains: to the west and to the east of the Cape Agulhas. The edge of the continental margin to the west of Cape Agulhas descends to depth of about 4000 m towards the seafloor. The upper margin is divided in three distinct morphological zones, namely, the inner-shelf; middle shelf; and the upper slope. The inner-shelf is rocky, with widths varying between ~~10 (~~16 km~~)~~ and ~~20 miles (~~32 km~~)~~ between Cape Point and near Cape Agulhas, respectively. The middle shelf is gentle ~ 1 m km^{-1}, but it steepens at the out shelf towards the shelf-break. The shelf-edge varies from 200 to 400 m between south of Cape Agulhas and Cape Point respectively. The upper slope is characterized by a steeper average gradient of about 40 m km^{-1}. It encompasses some submarine canyons below the shelf-break. The Agulhas Bank is surrounded by important large-scale oceanographic features, namely, the warm Agulhas Current ~~on~~ along the south and east coast of South Africa, which derives its water from the Indian Ocean, and the cold Benguela Current ~~on~~ along the west coast which derives its water from the Atlantic Ocean (Lutjeharms, 2006).

Commented [M7]: Confusing "Cape Mountains"? Please clarify.

Along the east coast of South Africa, the continental shelf varies only between 3 and 16 km in width, stretching nearly in a sinuous fashion for about 724 km, between Port Elizabeth and Durban (Fig. 2b). In Durban the shelf widens for nearly 45 km and form is the Natal Bight (Fig. 2b). The wider shelf lies seaward of two trending coastal faults. After the Bight the continental shelf narrows again for about 6 km, heading north toward Maputo in Mozambique (Fig. 2c) nearly in a straight line, parallel with the inland Lebombo ~~chain of~~ Mountain~~s~~ chain located 80 km from the coast (Pepper and Everhart, 1963), especially between north of Cape St. Lucia and Maputo Bay.

~~*4.1.2.*~~ *Mozambican continental shelf*

In Maputo Bay (Fig. 2c) the shelf widens again and shallows forming one of the largest coastal indentations in the southwest Indian Ocean, the Delagoa Bight (Lamont et al., 2010; Lutjeharms and da Silva, 1988), ~~with~~ of about 64 km width (Pepper and Everhart, 1963). Pepper and Everhart (1963) attributed the greater widths of the Bight to ~~be related to~~ the accumulation of sediments deposited by a combination of two opposing currents at the bight, characterized by an intense southward flow field offshore and a weaker north-easterly flow inshore. Recent studies however suggest that the Bight hosts a semi-permanent cyclonic eddy, termed the Delagoa Bight eddy (Cossa et al., 2016; Lamont et al., 2010; Lutjeharms and da Silva, 1988). From the Bay the coast runs northward in a concave trajectory ~~fashion with reference to the sea~~ over a sandy ground toward Ponta de Barra, along a ~~variable~~ shelf ~~dimension~~ which varies from about 16 km to 74 km in width~~, being –~~ the latter possibly related to deposition and accumulation of sediments driven by a system of currents including an off-shore strong southward flow and a relatively weaker northward inner-shore flow around the Maputo Bay. From Ponta da Barra the coast progresses northward for about 217 km to the latitude of 22◦S, near the Bazaruto A~~a~~rchipelago. From Ponta da Barra to Bazaruto the shelf width narrows from about 16 km to 6 km at the offshore side of the island. Both at Ponta da Barra and south of Bazaruto, coastal embayments are formed, likely from the same geological process (Pepper and Everhart, ~~(~~1963).

From Bazaruto the continental shelf runs north~~-~~westward toward the broad shelf of Sofala Bank (Fig. 2d). There are shoal areas, likely to be coral reefs within the Bank, ~~likely~~ probably built ~~-~~up from sediments derived from several river streams flowing into the Indian Ocean (Fig. 2d). In this area, at the mouth of the rivers the shelf widens to about 145 km, near Beira. From the Zambezi Delta (Fig. 2d) to the narrows of the Mozambique Channel near 17◦S, along an extension of about 322 km, the continental

shelf varies from 64 km to 18 km. Across the Bank, transverse geological ~~fractures~~fractures, or faults ~~at~~ on the seafloor ~~on~~ off the coast and on the continental slope are evident, forming deep canyons (eg Zambezi canyon). Zambezi canyon extends south-eastward toward the Mozambique Basin (Fig. 1a). As characteriz~~s~~ed by Pepper and Everhart (1963), from the narrows of the Channel to the northern end of Mozambique (Rovuma River), the continental shelf is relatively narrow and irregular, ranging in width from 3 km to 24 km.

~~*4.1.3.*~~ *Tanzanian continental shelf*

From the Rovuma estuary to about 8°S lies a stretch of about 209 km along the coast of Tanzanian mainland (Fig. 2f), characteriz~~s~~ed by several cliffs and reefs. The narrow continental shelf closely follows the deep indentation of the coastline, and its width may not even exceed 5 km o~~i~~n average (Pepper and Everhart, 1963). However, around 8°S deep horizontal fractures across the seabed toward the coast and through the continental shelf are present. In the region neighbouring the fracture zone the continental shelf widens out considerably, ~~while roving~~ extending in a northeast orientation around Mafia Island (southernmost island of the Zanzibar archipelagos). From ~~the~~ northern Mafia Island, the continental shelf ~~heads up~~ tapers from about 72 km to 6 km along ~~a~~ the coral-rich stretch towards the Tanzanian mainland in a north-west direction~~, and its width varies from about 72 to 6 km, respectively~~. It is thought that sediment deposition from several rivers outflowing from the mainland to the west of Mafia have caused a seaward extension of the continental shelf in this area (Pepper and Everhart, 1963). From about 7°S to Dar es Salaam the continental shelf is narrow, but then it widens again ~~while trading~~ in a northeast orientation, progressing closely along the east coast of Zanzibar Island (Fig. 2f). Subsequently it bends on a northwest direction approaching the mainland at the opposite side of the Pemba Island (northernmost island of the Zanzibar A~~a~~rchipelago). Several small-scale indentations are present along the ~~seaside~~ western edge of the Pemba coastline. Excluding its northern and parts of the western sector, the continental shelf of ~~the~~ Pemba Island is very narrow. Excluding its northern entrance, the transect between Pemba and Tanzania mainland ~~the~~ reveals a continental slope that descends to depth of ~~about~~ between 549 m and 732 m across the ~~all~~ entire length of the Island. Whereas westward along a stretch of about 26 km the seafloor is flat, but it consistently upslopes toward the mainland continental shelf where it attains a width of about 10 km.

The stretch from the northern Pangani river in Tanzania towards the Tanzania-Kenya border (Fig. 2f), as well as the section between Dar es Salaam and Mombasa present geological faults of complex nature and sedimentations that appears to explain the origins and movement of the whole set of islands of the Zanzibar A~~a~~rchipelago (Fig. 2f).

Commented [M8]: Seems a reference should be included here.

~~*4.1.4.*~~ *Kenyan and Somalia continental shelves*

From the northeast coast of Kenya (Fig. 2f) to Somalia (Fig. 2g) the coast is generally very narrow, and predominantly rocky. There are few indentations and narrow beaches. The north-eastward continental shelf from Kenya to Horn of Africa in Somalia varies in width from place to place (Fig. 2g), between 19 and 48 km.

Commented [M9]: The widest area is north of Watamu where the North Kenya Bank, an offshore extension of the continental shelf extends 60 km from Ungwana Bay.

~~*4.1.5.*~~ *Madagascar continental shelf*

Directly east of Mozambique, roughly at a minimum distance of about 700 km lies the Island of Madagascar (Fig. 2e), ~~the fourth largest Island in the world. The Island has~~with a narrow continental shelf overall of about 24 km in width (Fig. 2e). In localiz~~s~~ed places however, it reaches a width of about 80.~~,~~5 km ~~in~~ on the s~~S~~outh coast, and 161 km on the northwest coast ~~of~~ at St. Andre. The Island has a nearly straight and narrow coastline along the east ~~coast~~, with some places (northeast ~~coast~~part) exhibiting an almost complete~~ly~~ absence of a continental shelf (Fig. 2e). The edges of the narrow continental shelf of the east coast are geological fault scarps, ~~and~~ with ~~its~~a slope that descends to depth

of about 1829 m~~, along an area of geological fault~~. In the western sector, the shelf extending from Morondava to Cape St. Andre hosts a series of small banks of corals reefs. The widest shelf surface, possibly harbouring some granites is located on the west coast, close to the Juan de Nova Island (Fig. 2d). From Cape St. Andre to Cape Amber the shelf average width is about 48 km, nevertheless it broadens further to the west of the Cape.

~~*4.1.6.*~~ *Seychelles Bank*

Seychelles Bank is a bathymetric feature of Precambrian granite basement, which lies in the western equatorial Indian Ocean, located on the northern extension of the Mascarene Plateau (Fig. 2h). The Bank is confined between 4◦S ~~–~~ 6◦S and 54◦E ~~–~~ 57◦E, and~~. The Bank~~ is shallow with nearly flat-topped shape at about 50 m depth below the sea-surface. It is characterized by an oval shape with a dimension of 400km by ~~×~~200 km long (Yossi, 1988). The slope edges of the Bank are steep, descending to depths of more than 3000 m, being an exception its southwestern and southeastern sectors, which descend to depths of about 2000 m and 1500 m respectively (Yossi, 1988). To the southwest, the Bank is connected to the Amirante Arc by ~~the~~ a 2000 m deep saddle ~~of about 2000 m~~ de~~pthep~~, while to the southwest it gets separated from the remaining Mascarene P~~p~~lateau by another ~~the~~ saddle also of about 2000 m depth.

~~5.~~ Mid-Ocean Ridge System

Mid-Oceanic Ridges are prominent, long extensions of mountain-like structures formed by tectonic plates in response to the convective processes in the mantle underneath the oceanic crust, creating magma material where the tectonic plates collide at a divergent boundary. In the Indian Ocean, such topographic relief is ~~composed~~ reflected by a system of three different ridges: Central Indian Ocean Ridge (CIR, Fig. 3a), Southwest Indian Ocean Ridge (SWIR, Fig. 3b), and Southeast Indian Ocean Ridge (SEIR, Fig. 3c). The ridge system is about 7×10^3 km long, and its western and eastern flanks rise from the seafloor for about 3×10^3 m (Parson and Evans, 2005). Along this length, the water depth is very variable. At its shallowest point it has been documented by Parson and Evans (2005) as being 1500 m ~~below the sea level~~, at about 66◦9′57″~~-~~E, 17◦30′22″~~-~~S. Whereas at its deepest point, it is the deepest in the world oceans, being about 5600 m around the SWIR. It is a system of ridges that divides the Indian Ocean seafloor into three different tectonic plates, separating (i) the Antarctica and Indian-Australian plate, (ii) the Arabian plate, and (iii) the East African plate, through three actively spreading plate boundaries. The ridge system meets at a triple point known as the Rodrigues Triple Junction (~ 25◦33S, 70◦E) nearly in the centre of the Indian Ocean. A brief characterization of these ridges is presented below.

Commented [M10]: Confusing. Please re-word.

~~*5.1.*~~ *Central Indian Ocean Ridge*

The Central Indian Ridge (CIR) is a very long feature that stretches from the Rodrigues T~~t~~riple Junction, going northward nearly on a meridional direction (Fig. 3a). After crossing the equator, it bends slightly to run along a north~~-~~westward direction into the Arabian Sea, where it joins the Carlsberg Ridge (Spencer et al., 2005). New oceanic crusts are known to be created along this ridge. Inspections on the segmentation and morphology of CIR using multibeam bathymetry and magnetic data over a stretch between 3◦S and 11◦S (Raju et al., 2012) suggests that CIR is slowly spreading with an average full spreading rate between 26 and 38 mm $year^{-1}$. On the stretch nearly between 20◦S and the E~~e~~quator, it reaches its highest elevation running through the remote volcanic islands of New Amsterdam and Saint Paul (Defant, 1961). While isolated from human interferences it has been documented that these islands are under threat from invasive alien fauna, flora and pollution brought about by the oceanic current system. As indicated before, the southernmost point of the CIR is at Triple Junction. From this point, running in a south~~-~~westward direction lies the ~~Southwest Indian Ridge (~~SWIR~~)~~.

~~*5.2.*~~ *Southwest Indian Ridge*

The SWIR is a prominent plate boundary that separates the African continent from ~~the~~ Antarctica (Fig. 3b), over 100 Ma, and has an extension of over 77 000 km, between Rodrigues Triple Junction and Bouvet Triple Junction at 55°S, 0.5°W (Bernard et al., 2005). It has been distinguished as the deepest ridge~~s~~ in the world ocean basins, and one that has an ultra-slow~~es~~t spreading rate, estimated in 15 mm $year^{-1}$ (Patriat et al., 1997). It consists of magmatic spreading segments alternated by amagmatic segments, obliquely oriented (Baines et al., 2007). The Ridge is also characterized by several transverse fractures of enormous width and depths range (Parson and Evans, 2005). It has been indicated that strong evidence exists supporting that SWIR can be divided in two parts: between 33 - 35°E and 35 - 43°E, exhibiting different spreading rates. From the Triple Junction running south~~-~~eastward ~~direction~~ lies the ~~South East Indian Ridge (~~SEIR~~),~~ ~~of which the details are~~ presented ~~in the next section~~below.

~~5.3.~~ *Southeast Indian Ridge*

Extending from the Rodrigues Triple Junction to Macquarie Triple Junction (63°S, 165°E), the SEIR (Fig. 3c) stretches for about 6000 km (Graham et al., 1999). Contrary to the SWIR, the SEIR has been described as the fastest spreading ridge~~s~~ when compared ~~against~~ to the SWIR and CIR (Royer and Schlich, 1988). Small et al. (1999) indicate its spreading rate~~s~~ rangesing between 59 - 75 km Ma^{-1}. It has been also inferred that this Ridge has the spreading memory of the movements of the Antarctica continent in relation to Australia and India since the late Cretaceous (Royer and Schlich, 1988). The SEIR is comprised~~s~~ of a variety of distinct morphology and segmentations. It is a primary place for basaltic magmatism, transporting the Indian Ocean Isotope in-print which is determined by its relatively high ratio 87Sr/86Sr, 207Pb/206Pb, and 208Pb/206Pb (Graham et al., 1999). SEIR runs through a rough topographic path, near islands (eg Kerguelen-Heard, Amsterdam, St. Paul), ridges (eg Ninety-East Ridge) and plateaus (eg Kerguelen).

As seen from Fig. 1, apart from the Mid-Ocean Ridge System, the WIO region is also further complexed by several other ridge~~s~~ structures. Along the meridional extension of the CIR there are two outlying ridges: t~~T~~o the east, being the Chagos-Laccadive Ridge (Fig. 3d), and to the west, the Mascarene Plateau (Fig. 3e), of which the descriptions are presented next.

~~5.4.~~ *Chagos-Laccadive Ridge*

The Chagos-Laccadive Ridge (CLR) is a notorious aseismic volcanic ridge in the northern Indian Ocean (Fig. 3d) that stretches along a north-south distance ~~(Fig. 3d)~~ of about 2000 km ~~long~~ (Parson and Evans, 2005)~~, heading southward~~. Starting from the southwest Indian continental shelf, it runs south, carrying the Chagos Islands, passing through the Maldives and Laccadive, thus providing to the Ridge three extending blocks, termed in the literature as the Southern, Middle and Northern blocks, which ~~depicts~~represents the Chagos, Maldives and Laccadive blocks respectively, with correspondence to continental, oceanic, and oceanic structures, respectively (Nair et al., 2013). The ~~Ridge~~ CLR is characterized by several fracture zones along its margins, with a north-south orientation, comprising an array of segments of different origins (Avraham and Bunce, 1977), of which some parts are volcanic while others are of continental origin rifted from India. It is important to ~~mention~~ note that ~~it is quite controversial in~~ the literature fails to ~~draw~~ present a conclusive agreement on ~~d information about~~ the actual origin of this Ridge, ~~as~~ with several authors ~~have~~ suggesting~~ed~~ different processes~~, which results~~and ~~in~~ contrasting ~~opinions~~explanations. The ~~Ridge~~ CLR ~~has been~~is described as being asymmetric ~~with~~ due to its eastern flank being steeper than the western one. The average depth of the ~~Ridge~~ CLR is known to be less than 1000 m ~~below the sea surface~~, comprising of coral atolls and volcanic islands (Nair et al., 2013). Observational drilling data supports the possibility that the northern portion of the CLR is thicker than a normal oceanic crust. This being true, then it has originated from a hotspot locus.

Commented [M11]: Unclear. Please re-word.

Commented [M12]: Does this need a reference?

~~5.5.~~ *Mascarene Plateau*

The Mascarene Plateau (MASP) has been referred in the literature as one of the most prominent shallow bathymetric features of the Indian Ocean (Parson and Evans, 2005). The ~~Plateau~~ MASP is crescent-

shaped, concaved to the east, stretching between 4◦S to 20◦S, between the islands of Seychelles and the Mauritius respectively, covering over a distance of about 2000 km (Fig. 3e). It is located nearly across a zonal stretch lying within 54◦E and 63◦E. The description presented by Defant (1961) infers that it comprises two shallow branches: the northwest branch that hosts the Seychelles (Fig. 2h), and the Amirante Islands, of which it is of the continental origins (Seychelles Archipelago), and the other branch to the southwest which is of volcanic origin that hosts the volcanic islands of Mauritius and Reunion (Fig. 2e). The Plateau MASP is replete ofsupports several shallow banks and, shoals, fractured by deep-reaching channels (∼ 1000––1500 m). The water depth over the banks can be as shallow as 20 m (New et al., 2005). They are floored by corals, and occasionally can out-crop the sea-surface to form small scale islands (New et al., 2007). The flanks of the plateau in some cases descend abruptly to depths of about 2000 to 3000 m, and in other cases it gently descends to depths of about 4000 m. New et al. (2007) indicates that between the Seychelles island and the Saya de Malha Bank exists a 400 km long topographic ridge below 1000––1500 m depth from the sea surface. Furthermore, New et al. (2007) also identify a narrow gap of 100 km between the banks of Saya de Malha and Nazareth, located between 12◦S and 13◦S, of which it deepenings to over 1000 m.

In addition, the description by New et al. (2007) also reveals the existence of a shallow and narrow channel near 16◦S, of about 200 m deep and less than 50 km wide between the Nazareth and Cargados-Carajos Banks. On the other hand, Bbetween the Cargados-Carajos Bank and Mauritius also exist two deep and narrow channels of about 2000––3000 m and of about 50 km wide respectively, along a meridional stretch between 18◦S and 19◦S. It is expected that this complex bathymetric configuration has strong implications on the hydrodynamic nature of the ocean circulation in the area.

5.6. Madagascar Ridge

A comprehensive characterization of the topographic structure of the Madagascar Ridge (MDR) can be found in the study by Goslin et al. (1980), from which this section is based upon. The MDR is an elongated topographic barrier, southward oriented (Fig. 3f), which stretches directly from the southern tip of Madagascar at about 26◦S, and terminates at about 36◦S (Fig. 1a), where it collides against the SWIR, covering a meridional distance of about 1300 km. It is extensively characterized by a localized complex assemblage of Precambrian to Holocene continental igneous and sedimentary rocks. The geometry of theis Ridge MDR suggests it has a maximum width of about 750 km at latitude of 32◦S (Goslin et al., 1980). Interestingly the latitude of 32◦S also sets the mark that divides the MDR in two distinct domains: tTo the north, more precisely to the north of 31◦S, it is characterized by small sediment-filled pockets between a number of basaltic sediment highs. In this part, the western sector of the Ridge MDR is delineated by large-scale normal faults. Whereas to the east, the late Cretaceous fracture zones of the Madagascar Basin advances with deep penetration into the RidgeMDR. To the South of 32◦S, it is characterized by an extensive region of thick undeformed sediments across the central part of the RidgeMDR. The maximum depths in the centre of the plateau ranges between 1500 and 2000 m, excluding localized seamounts or shoals where a minimum depth of 20 m has been observed over the Walter Shoal, situated on the southwestern portion of the ridge. Both the western and eastern flanks of the MDR are steep and descend to depths below 5000 m into the Mozambique and Madagascar Basins, respectively (Fig. 1a).

5.7. Mozambique Ridge

Details about the morphological characteristics and geological processes (magmatism and volcanism) occurring in the Mozambique Ridge (MZR) and its Basin has been published by Köning and Jokat (2010). The MZR is an elongated feature, nNorth-sSouth oriented, of about 1300 km long (Fig. 3g). It lies roughly parallel to the southeast coast of Africa (Fig. 1a), between the parallels of 25◦S and 35◦S, and meridians of 34◦E and 36◦E (Maia et al., 1990). The Ridge MZR is bound to the east by a deep, nearly linear scarp that steeply descends down into the Mozambique Basin, for more thanover 5000 m deep. Whereas to the west the flanks of the Ridge MZR descend gently ointo the bounds of the Transkei Basin, also known

as the Natal Valley (Fig. 1a, Fig. 2b). The MZR has been recently reclassified as being of oceanic origin (Köning and Jokat, 2010), and being comprised of~~s~~ several bathymetric plateaus ~~of~~ which rise from the seafloor to heights of about 3500 m (Köning and Jokat, 2010), leading to a shallow water depth over the ~~Ridges~~ MZR crest. Contrary to former conceptual descriptions, the tectonic model results presented by Köning and Jokat (2010) suggest that the present location (off southeast Africa) of the ~~Mozambique~~ MZR~~Ridge~~ has been determined by long-lasting volcanic activities during the initial phases of separation between the African continent and Antarctica (Fig. 1a).

~~5.8.~~ *Davie Ridge*

The Davie Ridge (DVR) is a shallow bathymetric feature located in the Mozambique Channel, between Mozambique to the west and Madagascar Island to the east (Fig. 3h). The ~~Ridge~~ DVR runs in a n~~N~~orth-s~~S~~outh orientation and is about 1200 km long (Müller, 2017). The water level above the ~~Ridge~~ DVR is variable, where shallowest depth observed is 20 m over the Mount Saint Lazare. The ~~Ridge~~ DVR shows an asymmetric profile, with its western flank progressing steeply than its eastern flank, which shows relatively a gentle incline. This n~~N~~orth-s~~S~~outh orientation has a strong impact on the hydrodynamic regime of the bottom water circulation and sediment transports within the Mozambique Channel (Wiles, 2014). The ~~Ridge~~ DVR has been described as a curvilinear fracture zone that facilitated the southward drift of Madagascar away from the African main continent between the late Jurassic and early Cretaceous geological scales (Bassias, 1992).~~–~~ It separates two important oceanic basins: Mozambique Basin to the south and Somalia Basin to the north (Fig. 1a).

~~6.~~ Deep Ocean Channels and Ocean Basins

The seafloor topography of the WIO hosts seven major deep ocean basins (Fig. 1a), namely, Arabian Sea Basin (ASB), Somali Basin (SMB), Central Indian Basin (CIB), Mascarene Basin (MSB), Madagascar Basin (MDB), Mozambique Basin (MZB), and Crozet Basin (CZB). Each of these have been formed by distinct geologic process (origins), that give them different geologic patterns (Fig. 1a).

Formatted: Justified

Formatted: Font: Not Italic

~~6.1.~~ *Mozambique Channel*

The channel lies between the coast of Mozambique on the west side and the west coast of Madagascar to the east (Fig. 1a, Fig. 2d). The northern end of the channel ~~is~~ extends from the Rovuma estuary (10°28′S and 40°26′E) to Ras-Habu, at the northern point of Comoro Islands (Fig. 1a, Fig. 2e), to the northern tip of Madagascar at Cape Amber (11°57′S, 49°17′E). The southern boundary stretches from Ponta do Ouro in southern Mozambique mainland (26°53′S, 32°56′E) to Cape Sainte-Marie, at the southern tip of Madagascar (Fig. 2e).

~~The seafloor topography of the western Indian Ocean hosts seven major deep ocean basins (Fig. 1a), namely, Arabian Sea Basin (ASB), Somali Basin (SMB), Central Indian Basin (CIB), Mascarene Basin (MSB), Madagascar Basin (MDB), Mozambique Basin (MZB), and Crozet Basin (CZB). Each of these have been formed by distinct geologic process (origins), that give them different geologic patterns (Fig. 1a).~~

~~6.2.~~ *Arabian Basin*

The Arabian Basin is a submarine basin of the southern Arabian Sea (Fig. 1a), which rises toward the submerged Carlsberg Ridge to the south, the Maldive Islands to the southeast, India and Pakistan to the northeast, Iran to the north, and the Arabian Peninsula to the west. The Basin has a maximum depth of about 5~~,~~875 m and is separated by the Carlsberg Ridge from the deeper Somali Basin to the south and west. The sill depth between the Arabian and Somali Basins is 3~~-~~000 m. The floor of the basin, except along the southeastern edge, is covered by sediment deposited by the Indus River in the form of a large alluvial fan. The northern Arabia Sea is dated by 40 Myr.

~~6.3.~~ *Somali Basin*

Somali Basin is a submarine basin located on the southwestern sector of the Arabian Sea, in the tropical northwest Indian Ocean, to the east of Somalia (Fig. 1a). The Carlsberg Ridge separates the Basin from the shallower Arabian Basin to the northeast. The Basin connects with the Mascarene and Madagascar Basins to the south, with sill depths of more than 3,600 m. The deepest sections of the Basin are about 5,100 m, and the seafloor is dated by to 66 Myr (Parson and Evans, 2005).

6.4. Mascarene Basin

On its northern part, the Mascarene Basin lies between Madagascar and the Seychelles Plateau in the north-west Indian Ocean (Fig. 1a). At its north western-most part, it is defined by the complex ridge trench Amirante Arc (Mason, 1984). To the south it connects to the Madagascar Basin. The Basin has depths of about 5,000 m, with deep floor areas aged to 76 Myr (Parson and Evans, 2005).

Commented [MC13]: Not in the references list

6.5. Madagascar Basin

The Madagascar Basin lies to the east of the Mozambique Basin (Fig. 1a), and is bounded by the south-eastern coast of Madagascar and the Madagascar RidgeMDR in the western side, and to the east by the Mid-Indian Ridge. In the north it is limited by Mascarene plateau, while to the south it is limited by the Southwest Indian RidgeSWIR. The seafloor is relatively younger than that of the Mozambique Basin, being dated by to 75 Myr (Parson and Evans, 2005) and, characterizsed by sandy silt bottom sediments.

6.6. Mozambique Basin

The Mozambique Basin is located between South Africa and the Mozambique Ridge to the west and to the east by Madagascar and the Madagascar RidgeMDR (Fig. 1a). The Basin is relatively shallower in the north, at the southern entrance of the Mozambique Channel, and deeper in the south. Maximum depth of the Basin reaches depth beyond 5000 m at its southern entrance (Read and Pollard, 1998). Its bottom floor is dated by 110 Myr old (Parson and Evans, 2005).

Commented [MC14]: Not in the list of references

7. Oceanic and atmospheric processes in the western Indian Ocean

The oOcean and atmosphere form a dynamic coupled-system, with . There is a strong interaction between them through the upper boundary layer turbulent fluxes. We The processes in each of these environments cannot be fully understoodand the processes in each of these environments if we they are regarded them separately as independent entities.

7.1. Large-scale atmospheric circulation

The atmospheric circulation in the western Indian OceanWIO, and by extension the whole Indian Ocean, is unique when compared against that of the Atlantic and Pacific Oceans. Fig. 3 (Halo and Raj, 2020) shows windstress (vectors) and windstress-curl, $\nabla \times \tau$ (colours), monthly climatology derived from Scatterometer of the Ocean Winds product described by Risien and Chelton (2008). The product is gridded on 1/4°x1/4° mesh over the global ocean. It is known to resolve/reproduce small scale (mesoscale) features otherwise impossible in other wind products such as NECP re-analysis.

In the map (Fig. 4), positive (negative) windstress curl in the northern hemisphere represents the Ekman suction (pumping) phenomena. In the southern hemisphere the opposite holds. Ekman suction suggests water is pushed upward in the base of the Ekman layer, resulting in an upwelling event due to divergence at the sea-surface. On the other handConversely, Ekman pumping implies water being pushed downward from the base of the Ekman layer, resulting on downwelling event through the oceanic water column, due to convergence at the sea-surface. The upward and downward movement of the water column is generally translated by into the movement of the thermocline, which in the WIO region is located at depths levels identified by the isotherm of 20°C. Looking at the windstress in Fig. 4, it is evident that in the WIO region, a nitid marked contrast between the southern and northern Indian Ocean surface wind patterns is observed at latitude of 10°S. To the south, the winds are predominantly

easterly trade winds almost all year around, while to the north of that latitude the winds vary strongly seasonally due to the Indian monsoons (Schott et al., 2009).

A noticeable change of the windstress direction during the full course of the year is evident to the south of Madagascar, where winds change from northeasterly to easterly (Fig. 4). Former studies in the region have attributed this forcing as partially contributing to upwelling events in the region. In the central Mozambique Channel, the winds are predominantly southeasterly all year around, but considerable changes are observed on the strength of the windstress curl. It is mostly positive from July to November (Fig. 4g - k), and more negative from January to March (Fig. 4a - c).

Commented [M15]: References?

~~7.2.~~ Monsoons

Monsoons are seasonally reversing winds dominant in the north Indian Ocean, caused by the different warming rates of the earth's ~~-~~surface between the Indian Ocean and the highlands of ~~the~~ India~~n~~'s interior region. During the months of November to March (Fig. 4k to Fig. 4c), the winds blow from the India~~n's~~ landmass to the sea (n~~N~~ortheast m~~M~~onsoon, north Indian Ocean winter monsoon), and from May to September (Fig. 4e to Fig. 4i) they blow from the ocean toward the Asian continent (s~~S~~outhwest m~~M~~onsoon). The months of April (Fig. 4d) and October (Fig. 4j) are the period of the transitions between the monsoons and are known as inter-monsoons. In addition, the equatorial trade winds are exceptionally weak, and unsustained. Peculiarities in the proximities of the E~~e~~quator are further revealed from the fact that the near equatorial winds have their easterly component during the late winter to/or beginning spring only, while the westerlies are semi-annual during the transitional phase of the two monsoons (Schott et al., 2009). During these transitions, strong eastward equatorial surface jets known as Wyrtki Jets strike. This provides significant contribution to the onset of Indian Ocean climate mode of variability, such as Indian Ocean Dipoles (IOD).

~~7.3.~~ Large-scale oceanic circulation

The large-scale surface circulation in the ~~western Indian Ocean~~WIO is shown in Fig. 5 and Fig. 6. The former schematic suggests the direction of the flow field, and the latter indicates the intensity (speed) of the currents, computed from CNES-CLS9 dataset. The circulation pattern includes a complex system of currents and counter-currents dominating both the northern and southern hemisphere~~,~~ and are strongly influenced by the atmospheric wind system forcing. The main current structure is the westward South Equatorial Current (SEC), that originates its waters from the western Pacific Ocean in the form of the Indonesian throughflow (Fig. 5) and the recirculation of the subtropical anticyclonic gyre of the south Indian Ocean (Stramma and Lutjeharms, 1997). The SEC propagates westward carrying slightly more than 50~~-~~ ~~-~~55 Sv of volume transport between 10°S – 20°S, before it starts to split-off into two branches when crossing through the confines of the gaps between the banks of the Mascarene Plateau (New et al., 2007). On reaching the e~~E~~ast coast of Madagascar, near 17°S (Fig. 5), the branches of the SEC are fully decoupled into two opposing branches parallel to the Madagascar coast, and receive their individual identities, namely, South East Madagascar Current (SEMC) propagating southward carrying a volume of about 20 Sv (Schott et al., 1988), and Northeast Madagascar Current (NEMC) due north, transporting about 30 Sv (Chapman et al., 2003; Schott and McCreary, 2001; Schott et al., 2009). The latter, after passing the northern tip of Madagascar, creates horizontal shear at its southern edge interacting with the island's topography (to be discussed later). The b~~B~~ulk of the NEMC added to the northern remains of the SEC propagate westward toward Africa mainland along the latitude of 12°S.

On reaching the African continent the flow splits into another two branches (Fig. 5) with contrasting and distinct dynamical patterns over space and time-scales. The southward branch carries about 18 Sv of the volume transport and propagates discontinuously through the whole length of the Mozambique Channel in form of mesoscale eddies (De Ruijter et al., 2002; Ridderinkhof and De Ruijter, 2003; Halo et al., 2014a). ~~On the other hand~~Meanwhile, the northward branch transports about 15 Sv of the water

volume and flows continuously as East African Coastal Current (EACC) along the coasts of Tanzania and Kenya (Schott et al., 1988). The former merges with the flow spawned at the southern termination of the SEMC, at the southern tip of Madagascar, in the southern Mozambique Basin (Stramma and Lutjeharms, 1997). Subsequently they become important sources of water ~~sources~~ and variability ~~in~~to the Agulhas Current (Lutjeharms, 2006).

The Agulhas Current (AC) is one of the most intense western boundary currents of the global ocean, which transports on average about 70 Sv, and propagates with an average speed of more than 1.5 m s^{-1} (Lutjeharms, 2006). The vigorous nature of the AC in relation to all other currents in the WIO region also can be perceived from Fig. 6. The AC terminates at the southwestern most tip of the Agulhas Bank, where it revolves on itself and flows back into the southwest Indian Ocean in form of the Agulhas Return Current (Fig. 5 and Fig. 6), carrying about 55 Sv of water transport (Lutjeharms and Ansorge, 2001), which recirculates back into the southern Indian Ocean anticyclonic subtropical gyre.

The EACC along the coast of Kenya supplies ~~its water to~~ the Somali Current~~, which in this time propagates northward along the coast of Somalia (Tomczak and Godfrey, 1994)~~. However, this supplement is conditional, ie seasonally (monsoon) dependent (Tomczak and Godfrey, 1994; Schott and McCreary, 2001; Schott et al., 2009). During the s~~S~~outhwest m~~M~~onsoon, the EACC feeds the Somali Current, and the flow progresses northward, crossing the E~~e~~quator, and later at about 4°N, it bends eastward and propagates as the North Equatorial Countercurrent, that feeds the westward Southwest Monsoon Current (SWMC) in the Arabian S~~s~~ea. Whereas during the n~~N~~ortheast m~~M~~onsoon, the Somali Current propagates southward along the coast, and confronts the EACC at about 2°S - 4°S. This confluence of the currents induces an eastward flow that supplies water toward the South Equatorial Countercurrent (SECC). SECC is known to flow eastward all year around (this feature also can be traced in Fig. 5), simply exchanging its position with reference to the water column (deepening into the sub-surface during Southwest Monsoons, thus becoming an equatorial undercurrent). During this period the monsoon current in the Arabian S~~s~~ea propagates westward as the North Monsoon Current (NMC).

In the southern hemisphere, to the southeast of Madagascar near the latitude of 25°S, an intriguing shallow South Indian Ocean Countercurrent (SICC) flows eastward transporting about 21 Sv (Siedler et al., 2006; Palastanga et al., 2007; Siedler et al., 2009). This flow was discovered almost one decade ago only. More recently, to the southwest coast of Madagascar another current has been uncovered. This current flows southward parallel to the coast, and it has been termed South West Madagascar Current (SWMC, Ramanantsoa et al., 2018).

Perhaps the most important aspect to highlight in Fig. 6 is the importance of incorporating the long-term maps of mesoscale dynamic topography derived from satellite altimetry. The data portrays features of the circulation known to be in geostrophic balance. They are computed from the horizontal components of the momentum equation of the fluid dynamics, whereby the Coriolis force (associated ~~to~~ with the rotation of the earth) is in dynamic balance with the pressure gradient force, while all the other terms of the equation are assumed to play a negligible effect. From the patterns shown in Fig. 6, it is evident that most of the above~~-~~described surface features (Fig. 5) of the circulation in the WIO are in geostrophic balance. It is also interesting to highlight the presence of mesoscale features (eg Great-Whirl eddy off northern Somali coast; Mozambique Channel eddies and Agulhas rings, though with a relative weaker imprint; and the equatorial waves) in this large-scale time-averaged dataset of the mean flow.

~~*7.4.*~~ *Oceanic modes of variability*

The most dominant modes of climate variability in the Indian Ocean are~~:~~ t~~T~~he m~~M~~onsoons, the Indian Ocean Dipole (IOD), the Indian Ocean Basin-wide (IOB) warming and the El-Niño Southern Oscillation (ENSO) (Saji et al., 2006).

~~*7.4.1.*~~ *El-Niño Southern Oscillation~~ENSO~~*

Commented [MC16]: In the previous paragraph is mentioned "Southwest Monsoon Current (SWMC)". Is part of the reference? Or is it missing ") ("?

Commented [MC17]: Not in the list of references

Formatted: Font: Italic

ENSO is a natural phenomenon characterized by ~~a~~ strong warming and cooling events of the sea-surface on the eastern equatorial Pacific Ocean and changes in the zonal pressure gradient on the western equatorial Pacific, which gets phased with the annual cycle of the Pacific SST anomalies. It shifts the Pacific atmospheric convection eastwards, while intensifying at ~~on~~ the central-eastern equatorial region. This shift modifies atmospheric circulation remotely in the tropics and extra-tropics through an atmospheric wave adjustment mechanism. This anomalous warming enters the equatorial Indian Ocean and reaches the ~~western Indian Ocean~~WIO (Fig. 7a-c). Thus, the WIO regions warms ~~-~~up during the ENSO periods, with maximum temperatures being observed from March to May. However, there are different mechanisms responsible for this warming. The leading mechanism in the tropical southwest Indian Ocean differs from that observed in other regions of the basin. For example, in the tropical southwest Indian Ocean processes within the ocean interior dominate, while in the rest of the Basin surface fluxes dominate (Schott et al., 2009).

Anomalous atmospheric perturbations in the form of anticyclonic wind stress curl in the tropical east Indian Ocean (due to changes of the atmospheric Walker circulation), excites a downwelling of Rossby waves that propagate westward. Upon their arrival in the tropical southwest Indian Ocean (after many months) they force both deepening of the thermocline and warming of the sea-surface. In the WIO region, and by extension for the whole Indian Ocean, the most severe ENSO event occurred in 1997 (Westerberg and Christiansson, 1999). The WIO region experienced severe rainfall and flooding events which caused many deaths and displacement of thousands of people, while the eastern Indian Ocean experienced severe draughts, which led to many fires causing likewise loses.

~~7.4.2. IOD and IOB~~Indian Ocean Dipole and the Indian Ocean Basin-wide (IOB) warming

In response to the westerly equatorial wind forcing, the oceans respond by triggering accelerated flows in only few days (jets). In the equatorial Indian Ocean, these occur during the transitional phases of the monsoons. These Wyrtki Jets (Wyrtki, 1973) move warm equatorial surface waters eastward, pilling-up in the eastern Indian Ocean, resulting in increased sea-level and thickness of the mixed layer in the ocean interior, as it deepens the thermocline. However, in the ~~western Indian Ocean~~WIO, it generates cooling events due to the on-set of a shallower thermocline. Thus, these jets become key role players contributing to the onset of the IOD, by virtue of weakening or eliminating the upwelling along the coast of Sumatra (Schott et al., 2009).

IOD is a natural coupled ocean-atmosphere event that usually develops during the month of June, and reaches its maximum peak in October, caused by a strong seasonal variability of the monsoonal winds that favours the occurrence of Bjerknes feedback in the eastern Indian Ocean during the summer and fall seasons, which occasionally sets the developments of oceanic-atmospheric anomalies of similar nature of the La-Niña phenomenon (Schott et al., 2009). The cooling of the zonal equatorial gradient of sea-surface temperature is coupled with the shoaling of the thermocline. With the development of the IOD, a zonal east-west dipole of anomalous rainfall strikes the tropical Indian Ocean. Fig. 7d-f was computed from SST anomalies composites for the month of September (Wieners et al., 2019). IOD is characterized by a strong increase of rainfall event on the WIO region. The IOD also influences the intensity of the ocean currents depending on its positive or negative phase translated by a weakening or strengthening, respectively (Palastanga et al., 2006). During the IOD positive phase in 1994 and 1997 the measured ocean currents in the ~~Western Indian Ocean~~WIO, namely, the SEC, NEMC, SEMC, EACC and the eddy field in the Mozambique had weakened, whereas during its negative phase in 1996 and 1998 they had intensified (Palastanga et al., 2006).

Commented [M18]: Seems out of place. Does this explanation need to be here? Maybe link it to the place below where the figures are referred to, or to the figure legend.

The IOD, IOB and ENSO events are depicted in Fig. 7. The IOB is not further discussed here as its signal can be damped by the amplitude of the ENSO variability. Figure 7 was extracted from the work by Wieners et al. (2019)~~,~~ and ~~are~~ constructed from a set of observational datasets (Fig. 7, left panels) and numerical simulations by ~~a~~ the climate model the Community Earth System Model (CESM), in two experiments with different grid resolutions for the oceans and atmosphere. The higher resolution (HR)

is at 0.1° grid cell (Fig. 7, middle panels), and the lower resolution (LR) is at 1° grid cell (Fig. 7, right panels). The top panels (Fig. 7a – c) represents the peak of the ENSO, occurring during the month of December, and were computed from composite of SST anomalies. It is nNoticeable are the warm anomaly (in the Pacific Ocean) and the cold anomaly (eastern Indian Ocean) tongues. Figure 7, middle row (Fig. 7d - f) also shows the IOD event during its positive phase (September). It This plot has been computed from composite anomalies, also from observations, and HR and LR model simulations. The bottom panels represent the IOB distribution (Fig. 7g – i). Overall Fig. 7 highlights the level of interactions of the co-occurrence between ENSO and the positive phase of IOD events, and vice-versa (Wieners et al., 2019).

Commented [M19]: Somewhere here to incorporate the text mentioned in the above comment?

7.5. Mesoscale variability

Monthly climatological maps of sea level anomalies (SLA) for 24 years of observation, (1993 – 2016), over the full annual cycle period (January – December) areis displayed in Fig. 8. The daily data was gridded in a regular grid of 1/4°x1/4°, across the global ocean, on a daily basis. The dataset is produced by the French institutions: National Centre for Spatial Studies (CNES), Collecte Localis Satellites (CLS) and freely distributed on-line via the Copernicus Marine Services (http: //marine.copernicus.eu/).

The patterns in Fig. 8 reveal reflect a strong seasonality, with significant regional and local variabilities. Furthermore, it is also remarkable the differences of the geometrical structures represented by the closed contours of SLA are also remarkable. Larger and predominantly zonally elongated features dominate the northwest Indian Ocean, while a more circular geometric structures are dominanted in the southwest Indian Ocean. Overall, the northern Indian Ocean suggest stronger seasonal differences than the southern hemisphere. The same is true within the northern hemisphere itself between the eastern and western boundaries of the Arabian Basin.

On climatological timescales, from November to February, sea -level falls within the northeast monsoon period, during which a remarkable larger and intense lower (negative) SLA is positioned along the northern coast of Somali (Fig. 8k, l – a), exactly where the Great Whirl eddy develops and resides (see Fig. 6). This pattern shifts to a strongly higher (positive) SLA from May to September (Fig. 8e – i) when the winds are from southeast (see Fig. 4). These patterns are consistent with positive windstress curl adjacent to the northern Somali coast which results in surface divergence and Ekman driven upwelling during the northeast monsoon, conversely which in turn gives way to surface convergence thus downwelling during the southeast monsoons.

A remarkable feature worthy to of highlighting on Fig. 8, in the greater Agulhas system, is the seasonality on the strength of the SLA. Higher SLA have been observed from November to March (Fig. 8k – c), and lower SLA have been observed from April to October (Fig. 8d – j).

Today it has been well established that the dominant patterns observed in Fig. 8 represents both westward propagating mesoscale eddies (Schouten et al., 2002a; Quartly et al., 2006) and planetary Rossby waves (Schouten et al., 2002a; De Ruijter et al., 2005; Palastanga et al., 2007), whereby the former prevails the most (Quartly et al., 2006).

7.5.1. Eddies

Mesoscale oceanic eddies are turbulent circular rotating flows in the ocean, characterized by a typical time-scale of about 10 to 90 days, and typical space-scale between 10 to 500 km (Robinson, 1983). They can be generated by different physical processes, such as barotropic and baroclinic instabilities of the flow field. In fact, eddies are ubiquitous features in the global ocean. They are the most vigorous mesoscale processes. Many can be found in the southwest Indian Ocean, especially to the south of about 10◦S.

Attempt to map eddies in the WIO Basin as a whole, a domain which combines three large Marine Ecosystems (LME), namely the Agulhas Current LME, the Somali Coastal Current LME and the Red Sea LME was conducted recently by Halo and Raj (2020), using 20 years (1993 – 2012) of satellite altimetry dataset. By applying an automatic eddy detection algorithm as described by Halo et al. (2014a), eddies were identified and tracked in time and space from 1 January 1993 to 31 December 2012, on a daily basis. Their generation sites and trajectories are shown in Fig. 9 (Halo and Raj, 2020). The red colour indicates anticlockwise rotating eddies and blue clockwise rotating. Only eddies with a lifetime equal and greater than 90 days have been presented. The bold dots indicate the generation sites and the end of the trajectory lines indicate their sites of decay.

Statistical census on the eddy field conducted by Halo and Raj (2020) reveals different spatial/temporal distribution patterns between the northwest and southwest Indian Ocean sectors, separated by a strong eddy desert region between 12°S and 3°N. Many mesoscale structures in this latitude band have relatively short lifespans, ~~lived~~ less than three months. Geometrical patterns of sea level anomalies in such a band (Fig. 8) suggest their identity as baroclinic Rossby waves (Halo and Raj, 2020).

Overall, more cyclonic than anticyclonic eddies were found, and all tracked structures exhibited a predominant westward and southwestward propagation, which were heavily impacted by the seabed morphology, continental land masses, islands and bathymetric ridges. These highlight the role that bottom topography plays in influencing oceanographic circulation processes ~~of the circulation~~. The eddy trajectories (Fig. 9) strongly suggest an effective inter-basin telecommunication which could potentially favour connectivity pathways of oceanic materials. The eddies also play a noticeable role on the distribution of surface chlorophyll, especially in coastal upwelling dominated areas (see Fig. 10). Given their strong nonlinear characteristics (Halo et al., 2014b; Halo and Raj, 2020) and their ability to circulate through different ocean basins in the region, it is thus expected that these eddies are important vectors of biological connectivity between different ecosystems within the Agulhas Somali Currents LME region.

When the SEC or NEMC passes at the northern tip of Madagascar some eddies are formed by barotropic instability (Biastoch et al., 1999; Halo, 2012). This is a physical mechanism or process whereby the energy from the mean currents are converted into a kinetic turbulent energy. Similar processes take place in the narrows of the Mozambique Channel (De Ruijter et al., 2002; Schouten et al., 2003). O~~I~~n average, four to six~~4–6~~ eddies are generated and pass through the Mozambique Channel ~~per~~ each year. They are highly energetic, and propagate through the full length of the Channel, with average speed of about 3.5 km day^{-1}. They rotate anticlockwise (anticyclonic)~~,~~ and are relatively warmer than their homologous counterparts that rotate clockwise (cyclonic). Hydrographic measurements across some of the anticyclonic eddies in the Mozambique Channel revealed that they are about 400 km wide, and reach the seafloor, in some cases deeper than 3000 m (De Ruijter et al., 2002; Ridderinkhof and De Ruijter, 2003). Similarly, at the southern tip of Madagascar, eddies and dipoles are also formed at the southern termination of the SEMC (De Ruijter et al., 2004; Quartly et al., 2006; Ridderinkhof et al., 2013; Halo et al., 2014b).

The Mozambique Channel ~~eddies and~~ eddies and dipoles interact among themselves, ~~causing~~ at times merging ~~and~~ or ~~some~~ decaying in the southern Mozambique Channel (De Ruijter et al., 2004; Quartly and Srokosz, 2004). Nevertheless, they move downstream with the Agulhas Current. During their southward excursion they occasionally interact with the main current, causing instabilities on the patch of the Agulhas Current (Lutjeharms, 2006), causing the current to move slightly offshore, thus generating a large cyclonic meander inshore of the Agulhas Current, termed the Natal Pulses (Lutjeharms and da Silva, 1988). The process is more frequently observed in the Natal Bight, because of the change of the continental shelf observed in the region. Several cyclonic eddy structures have been observed along the southeast coast of South Africa, ~~at the~~ inshore of the Agulhas Currents, such as the Durban eddies and break-away eddies in Algoa Bay (Gustella and Roberts, 2016). Eddies also are formed further downstream at the Agulhas Retroflection region (Fig. 9). These Agulhas rings transport heat and

salt into the south Atlantic Ocean, where~~by~~ it is thought ~~that~~ they play a crucial role ~~for the~~influencing the climate (Biastoch et al., 2009; Beal et al., 2011). Several eddies and meanders are also formed along the path of the Agulhas Return Current, formed either from the interaction of the current with the seafloor topography, and/or from the strong meridional thermal gradient across the Subtropical front. Some eddies are also formed from baroclinic instabilities.

Along the coasts of Tanzania, Kenya and Somalia, the mesoscale oceanic variability is dominated by relatively fewer eddy structures (Fig. 9), but with strong presence, especially during the southwest m~~M~~onsoon. During this period the Somali Current that received water supply from the EACC turn offshore after crossing the 4◦S, remnants of the flow re-circulates around the E~~e~~quator and form~~s~~ the eddy-like structure termed the Southern Gyre (see also Fig. 6). The gyre is relatively large (about 400 km wide) and shallow (about 100 to 300 m de~~p~~p~~th~~), ~~it~~ and has been reported to have its first appearance in the upper ocean in early June, ~~and it is~~being triggered ~~from~~ by instabilities of the northward flowing Somali Current, during the s~~S~~outhwest monsoon~~s~~. According to Gamoyo et al. (2017), the northward migration of the Southern Gyre is intensified by the arrival of downwelling energy pulses from the large-scale Rossby-waves coming from the far flanks of the east Indian Ocean. A closer look into Fig. 10 also reveals higher chlorophyll concentration around or/within the Southern Gyre.

Further north, another structure is formed, termed the Great Whirl (see Fig. 5 and Fig. 6). Even more north a third mesoscale feature is formed in Socotra, termed the Socotra eddy (Bruce and Beatty, 1985; Schott et al., 2009). It has been indicated that the Socotra eddy is persistently observed in many summer monsoon regimes, northeast of Socotra (Schott et al., 2009). Average climatology of the SSH anomalies presented in Fig. 8, as well as the map of eddy detection generation sites in Fig. 9 seems to corroborate this hypothesis.

~~7.5.2.~~ *Coastal shelf dynamics and upwelling events*

Because of shallow bottom topography, strong local wind forcing, river discharges and tides the oceanography of the coastal shelf systems are to some extent different from that of the open ocean. Nevertheless, they are strongly connected. Some examples are presented below to help describe the ~~in this section may help the reader to appreciate such~~ main features~~details~~.

In Fig. 10 ~~we present~~ a satellite-~~-~~derived composite map of chlorophyll concentrations in the WIO region ~~captured~~ for the month of November 2016. ~~. It~~ depicts a typical scenario that highlights the synergy between physical forcing of the circulation and its associated biological response in the form of upwelling events. After their formation in the narrows of the Channel, the Mozambique Channel eddies and rings propagate southward parallel to the western boundary of the Channel (Halo et al., 2014a). Because of their large horizontal scale, along the Sofala Bank, located immediately to the south of the narrows of the C~~c~~hannel (see reference to Sofala Bank in Fig. 2d), where the shelf is broad and shallow, their influence on the shelf circulation is very strong (Fig. 10). Recently it has been investigated within a numerical modelling framework of the Regional Ocean Modelling Systems (ROMS). It has been found that when a mesoscale cyclonic eddy is present at the coast, a shelf current is observed following northward. Whereas when an anticyclonic eddy is present, the shelf current changes its direction and propagates southward. Therefore, the shelf current is controlled by the off-shore coastal flow (regular train of mesoscale eddies) (Malauene et al., 2018). It is likely that this shelf current is the same current associated to the Zambezi R~~r~~iver plumes investigated by Nehama and Reason (2015).

Tides also have a strong influence on the shelf dynamics over the Sofala Bank (Fig. 2d). Modelling studies by Nehama and Reason (2015) and Chevane et al. (2016) have shown that tides interacting with the Bank are important drivers of strong vertical mixing, able to bring cold deep waters to the ~~sea~~ surface. The Sofala Bank has been identified as a hotspot for internal waves. The Mozambique Channel eddies also have a strong influence on the on-set of the Delagoa Bight eddy (Cossa et al., 2016), off Maputo Bay (Fig. 2c).

Commented [M20]: Needs a little more narrative to link this short statement with the rest of the paragraph.

Downstream of the Mozambique Channel, as the Agulhas Current propagates south-westward along the East Coast of South Africa, parallel to the coast and, attached to the continental slope (Fig. 6), it induces strong shear instabilities that generate small-scale clockwise rotating vortices at the inshore edge of the Current, because of the lateral friction. A typical example of this type of process is the formation of the Natal Pulse in the Natal Bight (Lutjeharms and Roberts, 1988), along the coast of Durban, where the continental shelf widens (see Fig. 2b). Because of surface divergence occurring within the clockwise rotating vortices, for mass and volume conservation purposes, the dynamics within the vortex interior, waters are upwelled towards the sea-surface onto the shelf. These cold, nutrient-rich waters (Gustella and Roberts, 2016) provide the ingredients required for the phytoplankton growth (Lamont et al., 2014), thus enhancing blooms of biological primary productivity (Fig. 10).

Processes similar to the Natal Pulses have been documented in the region, and given other attributes such as Durban Eddies, Durban Break-Away eddies (Gustella and Roberts, 2016). The dynamics of these events occasionally become responsible to for flooding the Agulhas Bank with cold waters. In addition, local winds oin the western edge of the Agulhas Bank have been also identified as playing a contributing role ion the generation of coastal upwelling events in the region (Goschen et al., 2015; Roberts and Nieuwenhuys, 2016). Cross-shelf dynamics driven by topographic induced upwelling events in the region also contribute towards high chlorophyll concentrations observed in Fig. 10, along the east coast of South Africa.

Upstream of the Mozambique Channel the continental shelf along the coasts of Tanzania and Kenya is generally a narrow strip which exhibits relatively different morphology and width (Fig. 2f). As earlier discussed in this chapter, the shelf is relatively narrow in the south and wider in the north. Along the coasts of Tanzania and Kenya (Fig. 2f), the on-shelf circulation has not been investigated extensively due to limited data records at desirable spatial and temporal resolution. Efforts to generate scientific information oin the area comes from few numerical solutions of circulation models. Thus, reliable knowledge of the inner-shelf circulation is scanty. Studies such as those by Manyilizu et al. (2014) and Shigalla and Shaghude (2014) have addressed primarily the dynamics along the path of the main core structure of the EACC, which appears to run relatively far off-shore. The most comprehensive study about the channels and inner-shelf circulation for these regions can be assessed from the work by Nyandwi (2013), Zavala-Garay et al. (2015) and that of Mayorga-Adame et al. (2016). The laetter was based on an inter-annual simulation using ROMS, with a horizontal grid resolution of 4 km, especially configureFig.d for the coasts of Tanzania and Kenya for a period spanning from 2000 to 2007. The studies indicate that on approaching the shelf, the geostrophic circulation enters into an accelerating mode as it follows the isobaths. On the other handIn contrast, on the shelf (considered by the authorshere as the inner 100 m isobath) the circulation weakens as the flow experiences friction due to a the shallow bathymetry that slows down the deep flows, as well as nd the presence of the chain of islands (Pemba, Zanzibar and Mafia). The shelf circulation appears to be sensitive to the spatial and temporal scale variability of the main large-scale oceanographic feature, the EACC.

The EACC is known to flow northward all year around (Newell, 1959; Schott et al., 1988; Swallow et al., 1991; Shigalla and Shaghude, 2014), nevertheless it experiences modes of weaker and stronger regimes linked to the seasonal variation of the atmospheric wind field, expressed in terms of monsoonal winds (see Fig. 4). During the sSouthe- East monsoons and the two periods of the reversal of the monsoons (inter-monsoons), spanning from April to November, the EACC is stronger (with characterizsing velocities greater than 0.85 m s^{-1}), so is the shelf circulation (Mayorga-Adame et al., 2016). On the other hand, during the nNorthe- East monsoon, extending from December to March, the EACC is weaker (characteristic velocities below 0.75 m s^{-1}), due to the opposite direction of the surface wind forcing. Consequently, the northward shelf circulation between the Mafia and Zanzibar Islands is blocked (Mayorga-Adame et al., 2016), as the effect of the bathymetry becomes more pronounced (ie shallow channels). Since the Pemba Channel is very deep, when compared against the Zanzibar and Mafia Channels, the shelf circulation remains on its northward excursion, as the flow overpowers topographic

Commented [M21]: Not 200 m?

Commented [MC22]: Not in the references list

Commented [MC23]: Not in the references list as 1991– only 1988.

obstacles. The topographic effects on the circulation patterns during this period also is also well perceived, as inspections on the currents at the different southern entrances of the channels (ie southern gaps between the islands and the African mainland) show reveal different current speeds as they havecorresponding to different bathymetric depths).

Commented [M24]: Please review this section for improved clarity.

The effects of the chain of the island system along the coasts of Tanzania and Kenya (Fig. 2f) on the coastal circulation depends on the intensity of the EACC (see Fig. 6), the geometry of the coastline (Fig. 2f) and the depth of the channels between the islands and the mainland (Mayorga-Adame et al., 2016). The interaction of the EACC with the shallow bed topography and the island's coastlines are important mechanisms driving the reversal of portions of the northward EACC at the northern entrances of the cChannels. These southward flows within the cChannels appear to exhibit different behaviours: iIn the northernmost Island of Pemba this southward oriented shelf current is weaker, but with a persistent nature all year around. Along the Zanzibar Island the flow is relatively stronger, reaching the strongest velocities between December and March, of which is the period of the nNorthe East monsoons. The current-topography/coastline interaction are also driving mechanisms leading to the formation of small-scale oceanic eddies which rotates clockwise/anticlockwise, depending of the morphology of the coast. These locally generated eddies (see Fig. 9) have been described as exhibiting both permanent to semi-permanent regimes. At the southern entrances of the cChannels these eddies can block the intrusion of the EACC into the cChannels (Mayorga-Adame et al., 2016). These eddies also are the drivers of localizsed upwelling phenomena (Fig. 10), that occasionally cause cooling events over the continental shelf (Mayorga-Adame et al., 2016).

Further north, along the EACC, another mesoscale feature observed and recently inspected from numerical solution of ROMS in the climatological configuration set by Gamoyo et al. (2017) along the coast of Kenya and Somalia is the Southern Gyre (see Fig. 5b). It appears to be formed in early June near the sea surface and deepens between 100 m – 300 m below the sea surface, as a result of instability in the northward flowing Somali Current. The gyre has a mean diameter of about 400 km, and retains cool and fresh waters in its interior, derived from the SEC (Gamoyo et al., 2017).

7.6. Water masses in WIO region

Oceanic water masses are usually classified on the basis of their vertical distribution throughout the water column, and can be clustered in an upward direction as: surface, intermediate, deep, bottom and abyssal waters (Defant, 1961).

Because of its relatively small geometry, the Indian Ocean has a complex upper water mass structure, mostly due to several factors such as: its enclosure by the Asian continent at the subtropics (Fig. 5), the regime of the monsoonal winds (Fig. 4) which control the dynamics of the currents on the upper layers in the northern Indian Ocean (Fig. 5, Fig. 6, Fig. 8), and the unbalanced rates of precipitation/evaporation between the eastern and western Indian OceanWIO (Wyrtki, 1971; Tomczak and Godfrey, 1994; Schott et al., 2009).

Figure 11 shows monthly means (January to December) of air-sea density fluxes, computed from haline and thermal fluxes at the sea surface (Howe, 2008). It depicts oceanic density gains (losses) portrayed by the positive (negative) fluxes on climatological time scales. Positive (negative) fluxes are indicative of cooling (heating) of the sea surface. Comparison between these fluxes and monthly mean climatology of SLA (Fig. 8), suggests a weakening pattern of the SLA signals in the greater Agulhas system during the periods of strong positive density fluxes, indicative of strong surface cooling events, especially observed between May (Fig. 11e) and August (Fig. 11h).

The imprint of the ocean-atmosphere density fluxes is closely related to the local hydrology, notably on precipitation and evaporation rates (Howe, 2008). Therefore, it has a strong influence on the formation and characteristics of the dominant water masses locally generated. The description of the WIO's main

water masses is presented in the section below. ~~For their references the reader is directed to the T/S diagram shown in Fig. 12, adapted from Beal et al. (2006), and Halo et al. (2017).~~

Commented [MC25]: Not in the references list

~~*7.6.1.*~~ *Upper waters*

At the surface and sub-surface layers (0 - 500 m depth), the s~~S~~outh-west Indian Ocean is mainly occupied by tropical and subtropical water masses (Fig. 12). The tropical surface water (TSW) is originated close to the equatorial band, ~~at~~ in the central Indian Basin. Its formation is related to both the excessive rates of precipitation over evaporation in the tropics (Wyrtki, 1971; Toole and Warren, 1993) and the influence of the low salinity waters of the Indonesian Throughflow, also referred as the Australasian Mediterranean Sea Waters (AAMW) (Tomczak and Godfrey, 1994). The TSW is characterized by salinity values lower than 35.~~,~~5 ppt and a neutral density ~~smaller~~ less than 25.~~,~~5 kg m^{-3} (Beal et al., 2006). Specific values of salinity and temperature range between 34.~~,~~91 and 35.~~,~~31 ppt, and between 24.~~,~~7◦C and 26.~~,~~3◦C, respectively (Donohue and Toole, 2003). The TSW enters in the subtropics via the branches of the South Equatorial Current (SEC) (Swallow et al., 1988; Schott et al., 1988), propagating along the east coast of Madagascar and along the east coast of Africa mainland (Fig. 5). The main route taken by the TSW during its southward spreading is made through the Mozambique Channel (Beal et al., 2006; Swallow et al., 1988).

At the sub-surface, or thermocline layers (200-500 m depth), the flow is mainly dominated by the subtropical surface water (STSW) and the AAMW (Fig. 12). The STSW is formed within the subtropical gyre of the south Indian Ocean, to the east of 90◦E (Wyrtki, 1971), and between latitudes 25◦S and 35◦S (Tomczak and Godfrey, 1994; DiMarco et al., 2002). Its formation is due to the excess of evaporation rates over precipitation. It is characterized by salinity greater than 35.~~,~~5 ppt and a neutral density range between 25.~~,~~5 kg m^{-3} and 26.4 kg m^{-3} (Beal et al., 2006). STSW is transported westward by the SEC and enters into the greater Agulhas system by the flow of the SEMC~~outh East Madagascar Current~~ (Beal et al., 2006). According to Donohue and Toole (2003), a distinction between TSW and STSW is made by a strong boundary between them, formed at about 28◦S, where it generates a sharp gradient of temperature and salinity.

The AAMW (Fig. 12) is originated in the tropics, from the Pacific Central Waters, and enters in the Indian Ocean through the Indonesian Throughflow (ITF) (see Fig. 5), between Timor and the islands to the east of Bali, and forms one of the strongest thermocline fronts of the world's ocean (Tomczak and Godfrey, 1994). It is characterized by temperatures between 8°C and 23°C, and salinities between 34.~~,~~4 and 35 ppt (Emery, 2001). Another subsurface water mass in the region is the SubA~~a~~ntarctic Mode Water (SAMW) (Fig. 12), formed at the subtropical convergence front, mainly between 46°E and 62°E (Fine, 1993), due to the winter cooling and deep convection (Fig. 11) to the south of the front (McCartney, 1977). It subducts into the thermocline and propagates northward into the subtropical gyre (Toole and Warren, 1993). The core of the SAMW is at about 500 m depth, ~~and~~ where it holds an oxygen maximum (DiMarco et al., 2002). To the north of about 28°S, the potential temperature and density of SAMW varies from 13°C and 26.~~,~~65 kg m^{-3} respectively at about 28°S, to values close to 11°C and 26.8 kg m^{-3} at 20°S (Donohue and Toole, 2003).

The zonal gradient of temperature, salinity and density along the southern Indian Ocean Basin, and the entrainment of the SAMW in the subtropical gyre results in a subtropical distribution of this water, with highest values of oxygen found ~~to~~ in the southeast Indian Ocean (Donohue and Toole, 2003). This extension is also termed South-East Indian Subantarctic Mode Water (SEISAMW)~~, and it is~~ characterized by a concentration of oxygen above 4.~~,~~9 ml l^{-1}, and a neutral density of 26.~~,~~8 kg m^{-3} (Wyrtki, 1971). This water mass enters into the WIO region through the westward branch of the subtropical gyre (Donohue and Toole, 2003). Similar to SAMW is the Indian Central Waters (ICW). The ICW is also originated in the subtropics and is characterized by temperatures ranging between 8°C and 25°C, and salinity between 34.~~,~~6 and 35.~~,~~8 ppt (Emery, 2001). Beal et al. (2006), has observed this water mass at a depth below the thermocline 300 m deep.

~~7.6.2.~~ Intermediate waters

At the intermediate layers, or below the thermocline waters (500 mm - 1500 m depth), the WIO is mostly occupied by the Antarctic Intermediate Waters (AAIW), in the southern hemisphere, and the Red Sea Waters (RSW) and the Arabian Sea Low Oxygen Waters (ASLOW) (Beal et al., 2006), in the northern hemisphere (Wyrtki, 1971) (Fig. 12). The AAIW is thought to be formed in the southeastern Pacific and enters into the Atlantic Ocean through the Drake Passage, and continues flowing eastward along the Subantarctic front (McCartney, 1977). Once in the Indian Ocean, at about 60°E, the AAIW flows northward into the subtropical gyre (Fine, 1993; Beal et al., 2006). However, it does not cross the 10°S latitude, because its propagation is blocked by the equatorial current systems (Tomczak and Godfrey, 1994). The fresher AAIW is characterized by a minimum in salinity ranging between 33.~~,~~8 and 34.~~,~~6 ppt, and temperature between 2°~~-~~C and 10°C (Emery, 2001).

~~On the other hand~~In contrast, the RSW is very saline (Fig. 12), being a~~. This~~ water mass ~~is~~ formed in the Red Sea Basin, ~~as a result~~from ~~of~~ excessive evaporation over precipitation, which leads to a sinking of surface waters in the Gulf of Aden (Wyrtki, 1971; Tomczak and Godfrey, 1994). This process induces a local formation of maximum salinity, ~~and minimum~~with reduced oxygen concentration (DiMarco et al., 2002). The RSW is characterized by a potential temperature of about 22°C, salinity of about 39 ppt, and a density of 27.~~,~~25 kg m^{-3} (Tomczak and Godfrey, 1994). It flows southwards, concentrated along the African coast, below the Zanzibar Current (Wyrtki, 1971; Beal et al., 2000; Donohue and Toole, 2003), and passes through the Mozambique Channel ~~and~~ eventually reaching~~es~~ the Agulhas Current (Beal et al., 2000; Donohue and Toole, 2003).

The ASLOW ~~is~~ originate~~sd~~ in the Arabian Basin and~~. This water mass~~ has been observed at about 1200 m depth (Beal et al., 2006). It ~~, and~~ is characterized by high values of salinity, a relatively lighter neutral density of 25.~~,~~5 kg m^{-3}, and low oxygen, less than 3.~~,~~8 ml l^{-1}. Such minimum oxygen concentrations are due to the high consumption rates associated to the seasonal high productivity. The ASLOW propagates southwards, concentrated along the western boundary of the Indian Ocean. During its journey it also enters ~~in~~ the Mozambique Channel. The ASLOW is a result of a mixing process between the Arabian Sea Water (ASW) and Bengal Bay Water (BBW). The ~~ASW~~ former is characterized by values of temperature ranging between 24°~~–~~C and 30°C, and salinity between 35.~~,~~5 and 36.~~,~~8 ppt; while the ~~BBW~~ latter is characterized by temperature ranging between 25°~~-~~C and 29°C, and salinity between 28 and 35 ppt (Emery, 2001).

~~7.6.3.~~ Deep and Abyssal waters

The deep layer of the Indian Ocean is filled by the Indian Deep Water (IDW). To the north of the E~~e~~quator this water mass is usually termed as the norther, or NIDW (Fig. 12), and in the south as the southern, or SIDW. To the north of 45°S this deep water mass ~~ranges~~ exists between 1500 and 3800 m depth, while to the south of this latitude it shallows to about 500 m depth (Tomczak and Godfrey, 1994). The IDW is characterized by a salinity greater than 34.~~,~~8 ppt in the western side of the Indian Ocean, and by 34.~~,~~75 ppt in its eastern side (Tomczak and Godfrey, 1994). It is formed in the Atlantic Ocean as a remaining part of the North Atlantic Deep Water that did not convert into the intermediate waters within the Atlantic sector. The IDW is carried eastwards by the Antarctic Circumpolar Current (ACC). In the South Indian Ocean, it propagates northwards, concentrated along the western boundary. On reaching the northern Indian Ocean, at the Somali Basin, this water mass flows eastwards, and upwells in the Arabian Seas and in the Bay of Bengal (Wyrtki, 1971). The deep circulation is below the permanent thermocline and is influenced by the inflow of the RSW and Persian Gulf Waters (PGW).

To the bottom, below 3800 m, the Indian Ocean is dominated by the Antarctic Bottom Water (AABW), also called Circumpolar Deep Waters (CDW). This water mass is characterized by a range of potential temperature between 1°C and 2°C, and salinity between 34.~~,~~62 and 34.~~,~~73 ppt (Emery, 2001). It is formed in the Southern Ocean and enters ~~into~~ the South-West Indian Ocean via the Mozambique and

Madagascar Basins (Fig. 1a), through the deep fractures of the South-West Indian Ocean Ridge, near 30◦S, and 56°E ~~–~~to 59°E (Tomczak and Godfrey, 1994). The flow in the Mozambique Basin is blocked within the Mozambique Channel by the Davie Ridge. In the Madagascar Basin (Fig. 1a), the water propagates further north and forms a western boundary current along the continental slope of the east coast of Madagascar.

In the southeast, this water mass enters ~~in~~ the Indian Ocean through the South Australasian Bight, around 50°S and 124°E (Tomczak and Godfrey, 1994). ~~In~~ To the south of Australia, it flows along the southern and western slope of Australia, and further north it escapes to the central Indian Ocean propagating along the eastern slope of the Ninetyeast Ridge (Tomczak and Godfrey, 1994). After crossing through the fractures of the Ridge, the water flows westwards and eventually reaches the northeast coast of Africa. Through the slope of the African continent it gradually upwells to form the North Indian Deep Waters.

~~8.~~ Acknowledgements

The author is grateful to the WIOMSA secretariat and UNEP/ Nairobi Convention for the trust for conducting this task. Gratitude is also extended to the anonymous reviewer who has helped to improve the quality of the manuscript, and to several data providers: Copernicus Marine Services for satellite altimetry data (EU); NCAR-National Science Foundation (US) for wind product, and World Ocean Atlas and National Oceanographic Centre (UK) for density flux dataset. Personal thanks to Dr. Nicolas Howe.

~~9.~~ Bibliography

Ansorge, I. and Lutjeharms, J. (2003). Eddies originating at the South-West Indian Ridge. *J. Mar. Sys.* 39, pp. 1–18. https://doi.org/10.1016/S0924-79639(02)00243-9

Avraham, Z.B. and Bunce, E.T. (1977). Geophysical study of the Chagos-Laccadive Ridge, Indian Ocean. *J. Geophys. Res.* 82 (8), pp. 1295–1305. https://doi.org/10.1029/JB082i008p01295

Baines, A.G., Cheadle., M.J., Dick., H.J.B., Scheirer, A.H., John, B.E., Kusznir, N.J. and Matsumoto, T. (2007). Evolution of the Southwest Indian Ridge from 55◦45'E to 62◦E: Changes in plate-boundary geometry since 26 Ma. *Geochem. Geophys. Geosys.* 8(6), Q06022. https://doi.org/10.1029/2006GC001559

Barlow, R.G., Marsac, F.S., Ternon, J.F. and Roberts, M. (2014). The Mozambique Channel: Mesoscale Dynamics and Ecosystem responses. *Deep Sea Res.*, Part II, 100, pp. 1-9. https://doi.org/ 10.1016/j.dsr2.2013.10.012

Bassias, Y. (1992). Petrological and geochemical investigation of rocks from the Davie fracture zone (Mozambique Chan- nel) and some tectonic implications. *J. Afr. Earth. Sci.* 15, pp. 321–339. https://doi.org/ 10.1016/0899-5362(92)90018-8

Beal, L.M., De Ruijter, W.P.M., Biastoch, A., Zahn, R., Cronin, M., Hermes, J., Lutjeharms, J., Quartly, G., Tozuka, T., Baker-Yeboah, S., Bornman, T., Cipollini, P., Dijkstra, H., Hall, I., Park, W., Peeters, F., Penven, P., Ridderinkhof, H. and Zinke, J. (2011). On the role of the Agulhas System in ocean circulation and climate. *Nature* 472, pp. 429–436. https://doi.org/10.1038/nature09983

Beal, M.L., Chereskin, T.K., Lenn, Y.D. and Elipot, S. (2006). The Sources and Mixing Characteristics of the Agulhas Current. J. *Phys. Oceanogr.* 36, pp. 2060–2074. https://doi.org/10.1175/JPO2964.1

Beal, M.L., Ffield, A. and Gordon, A.L. (2000). Spreading of the Red Sea Overflow waters in the Indian Ocean. *J. Geophys. Res.* 105, pp. 8549 – 8564. https://doi.org/10.1029/1999JC900306

Bernard, A., Munschy., M., Rotstein, Y. and Sauter, D. (2005). Refined spreading history at the Southwest Indian Ridge for the last 96 Ma, with the aid of satellite gravity data. *Geophys. J. Int.* 162, pp. 765–778. https://doi.org/ 10.1111/j.1365- 246X.2005.02672.x

Biastoch, A., Böning, C.W., Schwarzkopf, F.U. and Lutjeharms, J.R.E. (2009). Increase in Agulhas leakage due to poleward shift of Southern Hemisphere westerlies. *Nature* 462, pp. 495–498. https://doi.org/10.1038/nature08519

Biastoch, A., Riesen, C.J.C., Lutjeharms, J.R.E. and Boebel, O. (1999). The importance of flow in the Mozambique Channel to seasonality in the greater Agulhas Current System current. *Geophys. Res. Lett.* 26(21), pp. 3321–3324. https://doi.org/10.1029/1999GL002349

Bond, G. (1979). Evidence for some uplifts of large magnitude in continental platforms. *Tectonophysics* 61, 28–305. https://doi.org/10.1016/0040-1951(79)90302-0

Bruce, J.G. and Beatty, W.H. (1985). Some observations of the coalescing of Somali eddies and a description of the Socotra eddy. Oceanol. Acta 8(2), pp. 207-219

Cabral, P., Gabriela, A., Akandea, A., Costa, A., Amade, N., Niquisse, S., Atumane, A., Cuna, A., Kazemi, K., Mlucasse, R. and Santha, R. (2017). Assessing Mozambique's exposure to coastal climate hazards and erosion. *Int. J. Disaster Risk Reduction* 23, pp. 45-52. https://doi.org/10.1016/j.ijdrr.2017.04.002

Chapman, P., DiMarco, S.F., Davis, R.E. and Coward, A.C. (2003). Flow at intermediate depths around Madagascar based on ALACE float trajectories. *Deep Sea Res. Part II* 50(12-13), pp. 1957 – 1986. https://doi.org/10.1016/S0967-0645(03)00040-7

Chevane, C.M., Penven, P., Nehama, F.P.J. and Reason, C.J.C. (2016). Modelling the tides and their im- pacts on the vertical stratification over the Sofala Bank, Mozambique. *Afr. J. Mar. Sci.* 38, pp. 465–479. https://10.2989/1814232X.2016.1236039

Cossa, O., Penven, S.P.P., Capet, X. and Reason, C. J. C. (2016). Modelling cyclonic eddies in the Delagoa Bight region. *Clim. Dyn.* 39, pp. 509–529. https://doi.org/ 10.1007/s00382-011-1170-6

De Ruijter, W.P.M., Ridderinkhof, H., Lutjeharms, J.R.E., Schouten, M.W. and Veth, C. (2002). Observations of the flow in the Mozambique Channel. *Geophys. Res. Lett.* 29, pp. 1401–1403. https://doi.org/10.1098/rsta.2004.1478

De Ruijter, W.P.M., Ridderinkhof, H. and Schouten, M.W. (2005). Variability of the southwest Indian Ocean. Philos. *Trans. R. Soc. London A* 363, pp. 63–76. https://doi.org/10.1098/rsta.2004.1478

De Ruijter, W.P.M., van Aken, H.M., Beier, E.J., Lutjeharms, J.R.E., Matano, R.P. and Schouten, M.W. (2004). Eddies and dipoles around South Madagascar: formation, pathways and large-scale impact. Deep Sea Res., Part I 51, pp. 383– 400. https://doi.org/ 10.1016/j.dsr.2003.10.011

Defant, A. (1961). *A Physical Oceanography*. Vol. 1. Pergamon Press, New York, USA, 729 pp

DiMarco, S.F., Chapman, P., Nowlin, W.D., Hacker, P., Donohue, K., Luther, M., Johnson, G.C. and Toole, J. (2002). Volume transport and property distribution of the Mozambique Channel. *Deep Sea Res., Part II* 49, pp. 1481–1511. https://doi.org/10.1016/S0967-0645(01)00159-X

Donohue, K.A. and Toole, J.M. (2003). A near synoptic survey of the SouthWest Indian Ocean. *Deep Sea Res., Part II* 50, pp. 1893–1931. https://doi.org/10.1016/S0967-0645(03)00039-0

Emery, W.J. (2001). Water Types and Water Masses. *Encyclopedia of ocean sciences* 6, pp. 3179-3187. https://doi.org/10.1006/rwos.2001.0108

Fenta, A.A., Tsunekawa, A., Haregeweyn, N., Poesen, J., Tsubo, M., Borrelli, P., Panagos, P., Vanmaercke, M., Broeckx, J., Yasuda, H., Kawai, T. and Kurosaki, Y. (2020). Land susceptibility to water and wind erosion risks in the East Africa region. *Sci. Tot. Environ.* 703, p. 135016. https://doi.org/10.1016/j.scitotenv.2019.135016

Fine, R. (1993). Circulation of Antarctic Intermediate Water in the South Indian Ocean. *Deep Sea Res.* 40, pp. 2021–2042. https://doi.org/10.1016/0967-0637(93)90043-3

Gamoyo, M., Reason, C.J.C. and Collins, C. (2017). A numerical investigation of the Southern Gyre using ROMS. *J. Mar. Sys.* 169, pp. 11–24. https://doi.org/ 10.1016/j.jmarsys.2017.01.002

Goodman, S.M., Weyeneth, N., Ibrahim, Y., Saïd, Y. and Ruedi, M. (2010). A review of the bat fauna of the Comoro Archipelago. *Acta Chiropterologica* 12(1), pp. 117–141. https://doi.org/ 10.3161/150811010X504635

Goschen, W.S., Bornman, T.G., Deyzel, S.H.P. and Schumann, E.H. (2015). Coastal upwelling on the far eastern Agulhas Bank associated with large meanders in the Agulhas Current. Continental Shelf Research 101, pp. 34–46. https://doi.org/10.1016/jcsr.2015.04.004

Goslin, J., Segoufin, J., Schlich, R. and Fisher, R.L. (1980). Submarine topography and shallow structure of the Madagascar Ridge, western Indian Ocean. *Geol. Soc. Am. Bull.* 91(12), pp. 741–753. https://doi.org/ 10.1130/0016-7606(1980)91- 741:STASSO-2.0.CO2

Graham, D.W., Johnson, K.T.M., Priebe, L.D. and Lupton, J.E. (1999). Hotspot-ridge interaction along the Southeast Indian Ridge near Amsterdam and St. Paul islands: helium isotope evidence. *Earth Planet. Sci. Lett.* 167, pp. 297–310. https://doi.org/10.1016/S0012-821X(99)00030-8

Gustella, L. A. and Roberts, M.J. (2016). Dynamics and role of the Durban cyclonic eddy in the KwaZulu-Natal Bight ecosystem. ajms 38, S23–S42. https://doi.org/ 10.2989/1814232X.2016.1159982

Halo, I. (2012). The Mozambique Channel eddies: Characteristics and Mechanisms of formation. Ph.D. thesis, University of Cape Town

Halo, I., Backeberg, B., Penven, P., Ansorge, I., Reason, C. and Ullgren, J.E., (2014a). Eddy properties in the Mozambique Channel: A comparison between observations and two numerical ocean circulation models. *Deep Sea Res., Part II* 100, pp. 38–53. https://doi.org/ 10.1016/j.dsr2.2013.10.15

Halo, I., Penven, P., Backeberg, B., Ansorge, I., Shillington, F. and Roman, R. (2014b). Mesoscale eddy variability in the southern extension of the East Madagascar Current: Seasonal cycle, energy conversion terms, and eddy mean properties. *J. Geophys. Res.* 119, pp. 7324–7356. https://doi.org/10.1002/2014JC009820

Halo, I. and Raj, P.R. (2020). Comparative oceanographic variability during climate change in the Agulhas Current and Somali Coastal Current Large Marine Ecosystems. Env. Dev. endev-S-20-00428 (*in review*)

Harris, D.J. and Rocha, S. (2009). Comoros, pp177–180. In *Encyclopedia of Islands* (ed. R. G. Gillespie and D. A. Clague) xxxii + 1074 pp. University of California Press, Berkeley

Howe, N. (2008). The impact of air-sea fluxes on the thermohaline circulation. *Royal Met Soc.* 63(8), pp. 236 – 239. https://doi.org/10.1002/wea.277

Jung, G., Prange, M. and Schultz, M. (2016). Influence of topography on tropical African vegetation coverage. *Clim. Dyn.* 46, pp. 2535–2549. https://doi.org/10.1007/s00382-015-2716-9

Köning, M. and Jokat, W. (2010). Advanced insights into magmatism and volcanism of the Mozambique Ridge and Mozambique Basin in the view of new potential field data. *Geophys. J. Int.* 180, pp. 158 – 180. https://doi.org/10.1111/j.1365- 246X.2009.04433.x

Kruger, G.P. (1983). Terrain Morphology Map of Southern Africa. Soil and Irrigation Research Institute, Department of Agriculture.

Lamont, T., Barlow, G., Morris, T. and van der Berg, M.A. (2014). Characterization of mesoscale features and phytoplankton variability in the Mozambique Channel. *Deep Sea Res., Part II* 100, pp. 94–105. https://doi.org/10.1016/j.dsr2.2013.10.019

Lamont, T., Roberts, M.J., Barlow, R.G., Morris, T. and van der Berg, M. A. (2010). Circulation patterns in the Delagoa Bight, Mozambique, and the influence of deep ocean eddies. *Afr. J. Mar. Sci.* 32, pp. 553–562. https://doi.org/10.2989/1814232X.2010.538147

Leslie, A.D. (1991). Agroforestry practices in Somalia. *For. Ecol. Manage* 45, pp. 293-308. https://doi.org/10.1016/0378-1127(91)90224-J

Lutjeharms, J.R.E. (2006). *The Agulhas Current*. Vol. 1. Springer-Verlag, Berlin

Lutjeharms, J.R.E. and Ansorge, I. (2001). The Agulhas Return Current. *J. Mar. Sys.* 30, pp. 115–138. https://doi.org/10.1016/S0924-7963(01)00041-0

Lutjeharms, J.R.E. and Cooper, J. (1996). Interbasin leakage through Agulhas Current filaments. Deep Sea Res., Part I 43, 213–238. https://doi.org/10.1016/S0924-7963(01)00041-0

Lutjeharms, J.R.E. and da Silva, A.J. (1988). The Delagoa Bight eddy. *Deep Sea Res.* 35, pp. 619–634. https://doi.org/10.1016/0198-0149(88)90134-3

Lutjeharms, J.R.E. and Roberts, H.R. (1988). The Natal Pulse: an extreme transient on the Agulhas Current. *J. Geophys. Res.* 93, pp. 631–645. https://doi.org/10.1029/JC093iC01p00631

Maia, M., Diament, M. and Recq, M. (1990). Isostatic response of the lithosphere beneath the Mozambique Ridge (SW Indian Ocean) and geodynamic implications. *Geophys. J. Int.* 100(3), pp. 337–348. https://doi.org/10.1111/j.1365-246X.1990.tb00689.x

Malauene, B.S., Moloney, C.L., Lett, C., Roberts, M.J., Marsac, F. and Penven, P. (2018). Impact of offshore eddies on shelf circulation and river plumes of the Sofala Bank, Mozambique Channel. *J. Mar. Sys.* 185, pp. 1–12. https://doi.org/10.1016/j.jmarsys.2018.05.001

Manyilizu, M., Dufois, F., Penven, P. and Reason, C.J.C. (2014). Interannual variability of sea surface temperature and circulation in the tropical western Indian Ocean. *Afr. J. Mar. Sci.* 36 (2), pp. 233–252. https://doi.org/ 10.2989/1814232X.2014.928651

Matano, R.P. and Simionato, C. (1999). Modeling the Wind-Driven Variability of the South Indian Ocean. *J. Phys. Oceanogr.* 29, pp. 217–230. https://doi.org/10.1175/1520-0485(1999)029<0217:MTWDVO>2.0.CO;2

Mayorga-Adame, C.G., Strub, P.T., Batchelder, H.P. and Spitz, Y.H. (2016). Characterizing the circulation off the Kkenyan-T-tanzanian coast using an ocean model. *J. Geophys. Res.* 121, pp. 1377–1399. https://doi.org/ 10.1002/2015JC010860

McCartney, M. (1977). Subantarctic Mode Water, in: A voyage of discovery. *Deep Sea Res.* 24, (Suppl.), pp. 103–119.

Moore, A., Blenkinsop, T. and Cotterill, F. (2009). Southern African topography and erosion history: plumes or plate tectonics? *Terra Nova* 21, pp. 310–315. https://doi.org/ 10.1111/j.1365-3121.2009.00887.x

Müller, C.O. (2017). The Central Mozambique continental margin - Its tectonic evolution as the centrepiece of the initial Gondwana break-up. Ph.D. thesis, Alfred Wegener Institute, Bremen, Germany

Nair, N., Anand, S.P. and Rajaram, M. (2013). Tectonic framework of Laccadive Ridge in Western Continental Margin of India. *Mar. Geolog.* 346, pp. 79–90. https://doi.org/10.1016/j.margeo.2013.08.009

NationMaster (2018). Countries Compared by Geography - Terrain. International Statistics at NationMaster.com, CIA World Factbooks 18. NationMaster.com, http://www.nationmaster.com/country-info/stats/Geography/Terrain

Nehama, F.P.J. and Reason, C.J.C. (2015). Modelling the Zambezi River Plume. *Afr. J. Mar. Sci.* 37, pp. 593–604. https://doi.org/doi.org/10.2989/1814232X.2015.1113202

New, A.L., Alderson, S.G., Smeed, D.A. and Stansfield, K.L. (2007). On the circulation of water masses across the Mascarene Plateau in the South Indian Ocean. *Deep Sea Res., Part I* 54, pp. 42–74. https://doi.org/10.1016/j.dsr.2006.08.016

New, A.L., Stansfield, K.L., Smythe-Wright, D., Smeed, D.A., Evans, A.J. and Alderson, S.G. (2005). Physical and Biological Aspects of the Flow across the Mascarene Plateau in the South Indian Ocean. *Philos. Trans. R. Soc.* 363(1826), pp. 151–168. https://doi.org/10.1098/rst.2004.1484

Nyandwi, N. (2013). The effects of monsoons on the east African coastal current through the Zanzibar Channel, Tanzania. *J. Ocean Technol*. 8(No4), pp. 64–74

Oettli, P. and Camberlin, P. (2005). Influence of topography on monthly rainfall distribution over East Africa. *Climate Research* 28(3), pp. 199–212. https://doi.org/10.3354/cr028199

Palalane, J., Larson, M., Hanson, H. and Juízo, D. (2016). Coastal erosion in Mozambique: Governing processes and remedial measures. Coastal Erosion in Mozambique. *J. Coastal Res.* 32 (3), pp. 700–718. https://doi.org/10.2112/JCOASTRES-D-14-00020.1

Palastanga, V., van Leeuwen, P.J. and Ruijter, W.P.M.D. (2006). A link between low-frequency mesoscale eddy variability around Madagascar and the large-scale Indian Ocean variability. *J. Geophys. Res.* 111(C9) . https://doi.org/10.1029/2005JC003081

Palastanga, V., van Leeuwen, P.J., Schouten, M.W. and Ruijter, W.P.M.D. (2007). Flow structure and variability in the subtropical Indian Ocean. *J. Geophys. Res.* 112, C01001. https://doi.org/10.1029/2005JC003395

Parson, L.M. and Evans, A.J. (2005). Seafloor topography and tectonic elements of the Western Indian Ocean. *Philos. Trans. R. Soc.* 363(1826), pp. 15–24. https://doi.org/10.1098/rsta.2004.1472

Partridge, T.C., Dollar, E.S.J., Moolman, J. and Dollar, L.H. (2010). The geomorphic provinces of South Africa, Lesotho and Swaziland: A physiographic subdivision for earth and environmental scientists. *Trans. Roy. Soc. S. Afr.* 65(1), pp. 1 – 47. https://doi.org/ 10.1080/00359191003652033

Patriat, P., Sauter, D., Munschy, M., Parson, L. (1997). A Survey of the Southwest Indian Ridge Axis Between Atlantis II Fracture Zone and the Indian Ocean Triple Junction: Regional Setting and Large Scale Segmentation. *Mar. Geophys. Res.* 19, pp. 457–480. https://doi.org/ 10.1023/A:1004312623534

Penven, P., Lutjeharms, J.R.E. and Florenchie, P. (2006). Madagascar: a pacemaker for the Agulhas Current system? *Geophys. Res. Lett.* 33, L17609. https://doi.org/10.1029/2006GL026854

Pepper, J.F. and Everhart, G.M. (1963). *The Indian Ocean: The Geology of Its Bordering Lands and The Configuration of Its Floor*. Tech. rep., Department of the Interior United States Geological Survey

Pollard, R. and Read, J. (2017). Circulation, Stratification and seamounts in the Southwest Indian Ocean. *Deep Sea Res., Part II* 136, pp. 36–43. https://doi.org/ 10.1016/j.dsr2.2015.02.018

Quartly, G.D., Buck, J.J.H., Srokosz, M.A. and Coward, A.C. (2006). Eddies around Madagascar - The Retroflection re-considered. *J. Mar. Sys.* 63, pp. 115–129. https://doi.org/ 10.1016/j.jmarsys.2006.06.001

Quartly, G.D. and Srokosz, M.A. (2004). Eddies in the southern Mozambique Channel. *Deep Sea Res., Part II* 51, pp. 69–83. https://doi.org/ 10.1098/rsta.2002.1108

Raju, K.A.K., Samudrala, K., Drolia, R.K., Amarnath, D., Ramachandran, R. and Mudholkar, A. (2012). Segmentation and morphology of the Central Indian Ridge between 3◦S and 11◦S, Indian Ocean. *J. Tectonophys.* 554, pp. 114– 126. https://doi.org/10.1016/j.tecto.2012.06.001

Read, J. and Pollard, R. (2017). An introduction to the physical oceanography of six seamounts in the southwest Indian Ocean. *Deep Sea Res., Part II* 136, pp. 44–58. https://doi.org/ 10.1016/j.dsr2.2015.06.022

Ridderinkhof, H. and de Ruijter, W.P.M. (2003). Moored current observations in the Mozambique Channel. *Deep Sea Res., Part II* 50, pp. 1933–1955. https://doi.org/ 10.1016/S0967-0645(03)00041-9

Ridderinkhof, W., Le Bars, D., von der Heydt, A.S. and de Ruijter, W.P.M. (2013). Dipoles of the South-east Madagascar Current. Geophys. Res. Lett. 40(3), pp. 558-562. https://doi.org/10.1002/GRL.50157

Risien, C. and Chelton, D.B. (2008). A Global Climatology of Surface Wind and Wind Stress Fields from Eight Years of QuikSCAT Scatterometer Data. *J. Phys. Oceanogr.* 38, pp. 2379–2413. https://doi.org/10.1175/2008JPO3881.1

Roberts, M. and Nieuwenhuys, C. (2016). Observations and Mechanisms of upwelling in the northern Kwazulu-Natal Bight, South Africa. *Afr. J. Mar. Sci.* 38, pp. S43–S63. https://doi.org/ 10.2989/1814232X.2016.1194319

Robinson, A.R. (1983). *Eddies in Marine Science.* Springer-Verlag, 644 pp.

Royer, J. and Schlich, R. (1988). Southeast Indian Ridge Between the Rodriguez Triple Junction and the Amsterdam and Saint-Paul Islands: Detailed Kinematics for the Past 20 m.y. *J. Geophys. Res. Solid-Earth* 93(B11), pp. 13524–13550. https://doi.org/ 10.1029/JB093iB11p13524

Saji, H.N., Xie, S.P. and Yamagata, T. (2006). Tropical Indian Ocean Variability in the IPCC twentieth-century climate. *J. Clim.* 29(11), pp. 4397–4417. https://doi.org/10.1175/JCLI3847.1

Schott, F.A., Fieux, M., Kindle, J., Swallow, J. and Zantopp, R. (1988). The boundary currents east and north of Madagascar: 2 Direct measurements and model comparisons. *J. Geophys. Res.* 93, pp. 4963 – 4974. https://doi.org/10.1029/JC093iC05p04963

Schott, A.F., Xie, S.P. and McCreary Jr, J.P. (2009). Indian Ocean Circulation and Climate Variability. *Rev. Geophys.* 47, pp. 1–46. https://doi.org/10.1029/2007RG000245

Schott, F.A. and McCreary, J.P. (2001). The Monsoon circulation of the Indian Ocean. Prog. Oceanog. 51, 1–123.

Schouten, M. W., De Ruijter, W. P. M., van Leeuwen, P. J., 2002~~a~~. Upstream control of Agulhas ring shedding. *J. Geophys. Res.* 107, C83109. https://doi.org/ 10.1029/2001JC000804

Schouten, M.W., De Ruijter, W.P.M., van Leeuwen, P.J. and Ridderinkhof, H. (2003). Eddies and variability in the Mozam- bique Channel. *Deep Sea Res., Part II* 50, pp. 1987–2003. https://doi.org/ 10.1016/S0967-0645(03)00042-0

Sepulchre, P., Ramstein, G., Fluteau, F., Schuster, M.S., Tiercelin, J.J. and Brunet, M. (2006). Tectonic uplift and esatern africa aridification. *Science* 313, pp. 1419–1423. https://doi.org/10.1126/science.1129158

Shigalla, B.M. and Shaghude, Y.W. (2014). Modelling the dynamics of the Tanzanian coastal waters. *J. Ocean. Marine Science* 5(1), pp. 1–7. https://doi.org/10.5897/joms2013.0100

Siedler, G., Rouault, M., Biastoch, A., Backeberg, B., Reason, C.J.C. and Lutjeharms, J.R.E. (2009). Modes of the southern extension of the East Madagascar Current. *J. Geophys. Res.* 114, C01005. https://doi.org/ 10.1029/2008JC004921

Siedler, G., Rouault, M. and Lutjeharms, J.R.E. (2006). Structures and origin of the subtropical South Indian Ocean. *Geo- phys. Res. Lett.* 33, L24609. https://doi.org/ 10.1029/2006GL027399

Small, C., Cochran, J.R., Sempere, J. and Christie, D. (1999). The structure and segmentation of the southeast indian ridge. *Mar. Geolog.* 161, pp. 1–12. https://doi.org/ 10.1016/S0025-3227(99)00051-1

Spencer, T., Laugton, A.S. and Flemming, N.C. (2005). Variability, interaction and change in the atmosphere-ocean-ecology system of the Western Indian Ocean. *Philos. Trans. R. Soc.* 363, pp. 3–13. https://doi.org/ 10.1098/rsta.2004.1495

Stramma, L. and Lutjeharms, J.R.E. (1997). The flow field of the subtropical gyre in the South Indian Ocean into the Southeast Atlantic Ocean: A case study. *J. Geophys. Res.* 99, pp. 14053 – 14070. https://doi.org/10.1029/96JC03455

Swallow, J., Fieux, M. and Schott, F.A. (1988). The boundary currents east and north of Madagascar 1: Geostrophic currents and transports. *J. Geophys. Res.* 93, pp. 4951 – 4962. https://doi.org/10.1029/JC093iC05p04951

Tomczak, M. and Godfrey, J.S. (1994). Regional Oceanography: An Introduction. *Bull. Amer. Meteor. Soc.* 2, p. 390

Toole, J.M. and Warren, B.A. (1993). A hydrographical section across the subtropical South Indian Ocean. *Deep Sea Res.* 40 (10), pp. 1973–2019. https://doi.org/10.1016/0967-0637(93)90042-2

UMLP (2016). *World Regional Geography: People, Places and Globalization*. Vol. 2, ISBN: 978-1-946135-27-8. Minnesota Library Publishing. https://doi.org/10.24926/8668.2701

Formatted: Highlight

Westerberg, L.O. and Christiansson, C. (1999). Highlands in East Africa: Unstable Slopes, Unstable Environments? *Royal Swedish Academy of Sci,* 28, p. 5. In: Research for Mountain Area Development: Africa and Asia, pp. 419–429

Wieners, C., Dijkstra, H.A. and de Ruijter, W.P.M. (2019). The interaction between the western Indian Ocean and ENSO in CESM. *Clim. Dynamic* 52, pp. 5153-5172. https://doi.org/10.1007/s00382-018-4438-2

Wiles, E.A. (2014). Tectonic history, microtopography and bottom water circulation of the Natal Valley and Mozambique Ridge, southwest Indian Ocean. Ph.D. thesis, University of Kwazulu Natal, Durban, South Africa.

Wyrtki, K. (1971). Oceanographic Atlas of the International Indian Ocean Expedition. National Science Foundation.

Wyrtki, K. (1973). An equatorial jet in the Indian Ocean. *Sci.* 181, pp. 262–264. https://doi.org/10.1126/science.181.4096.262

Yang, W., Seager, R. and Cane, M. (2015). The annual cycle of east African precipitation. *J. Clim.* 28, pp. 2385–2404. https://doi.org/10.1175/JCLI-D-14-00484.1

Yossi, M. (1988). The Tectonic Setting of the Seychelles, Mascarene and Amirante Plateaus in the Western Equatorial Indian Ocean. *Mar. Geo.* 79, pp. 261–274. https://doi.org/10.1016/0025-3227(88)90042-4

Zavala-Garay, J., Theiss, J., Moulton, M., Walsh, C., Woesik, R., Mayorga-Adame, C.G., García-Reys, M., Mukaka, D.S., Whilden, K., Shaghude, Y.W. (2015). On the dynamics of the Zanzibar Channel. *J. Geophys. Res.* 120. https://doi.org/10.1002/2015JC010879

Zinke, J., Pfeiffer, M., Timm, O., Dullo, W., Kroon, D. and Thomassin, B. (2008). Mayotte coral reveals hydro- logical changes in the western Indian Ocean between 1881 and 1994. *Geophys. Res. Lett.* 35, L23707. https://doi.org/ 10.1029/2008/GL035634,2008

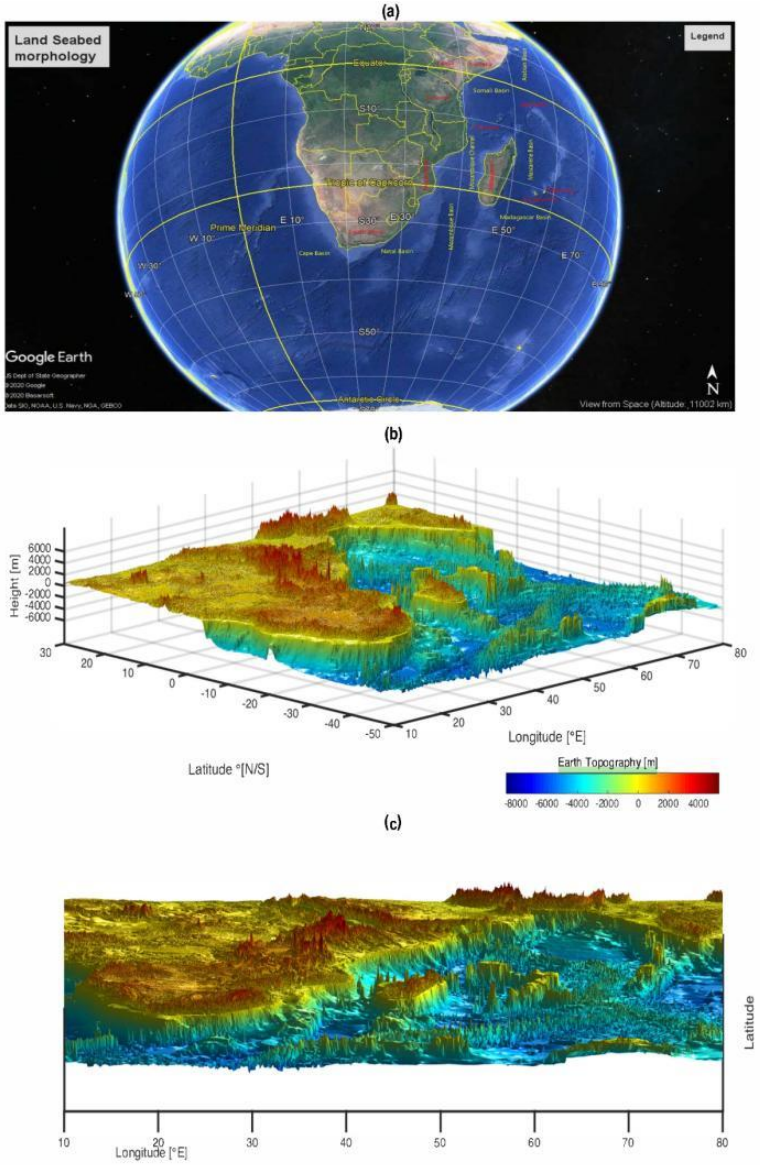

Fig. 1: Land-ocean bed morphology of the WIO region as derived from the GEBCO dataset. For better visualization, the topographic features in this panel have been reconstructed in a 3D frame, rotated by 5◦ Azimuthal angle and 60◦ elevation, using MATLAB software, then displayed in a horizontal flat plane. Note that the longitude and latitude values are not shown due to the rotational effects. The reader may find more informative to compare this plate with that shown in Fig. 5 with portrayal of the ocean currents. The background positive (negative) colours show~~s~~ the land (seafloor) topographic domains. The corresponding colour-bar is scaled in meters.

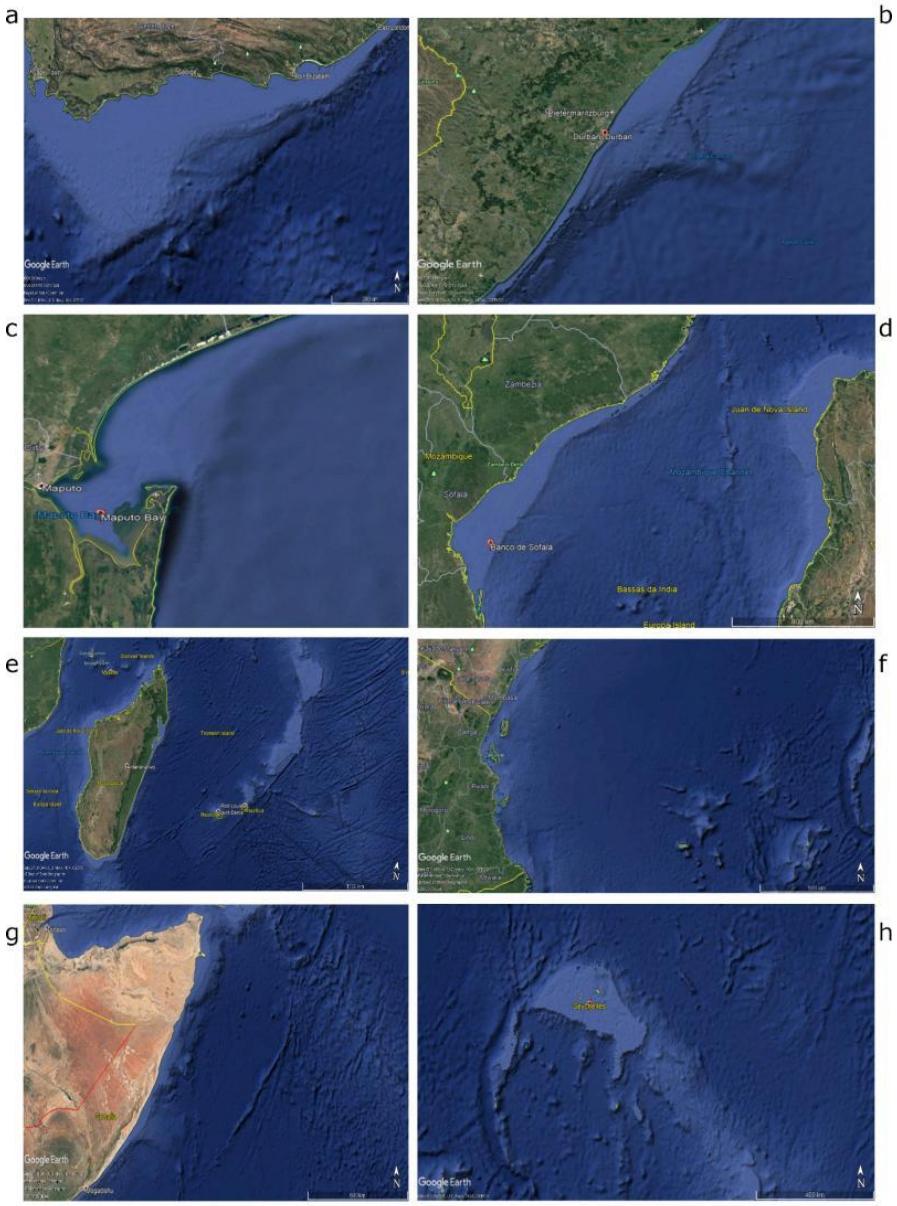

Fig. 2. Aerial view of the seabed morphology showing continental margins and main deep ocean basins in the ~~western Indian Ocean~~WIO. Special attention is made for the following features~~ are~~: (a) Agulhas Bank; (b) Natal Bight; (c) Delagoa Bight; (d) Sofala Bank and western Madagascar Bank; (e) Comoros archipelagos, Madagascar southern and eastern continental shelves, Mauritius and La-Reunion Islands, Mascarene Plateau; (f) Tanzanian and Kenyan continental shelves, including Mafia, Zanzibar and Pemba Islands; (g) Somali continental shelf and (h) Seychelles Island and its bank.

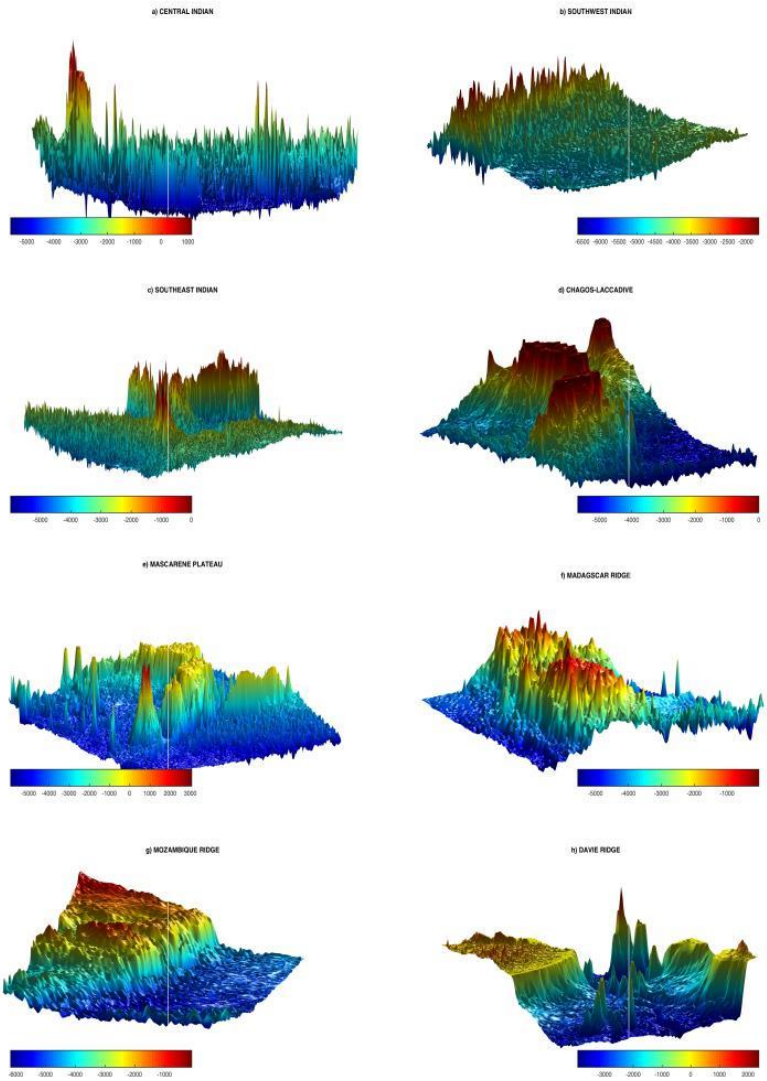

Fig. 3: Morphological profiles of the major oceanic ridges in the ~~Western Indian Ocean~~WIO region, discussed in this chapter. See the titles for better reference. Notice that the colour bar is not fixed for all the panels. It is not meant to compare them as in some cases the islands and parts of the continent are shown, whereas in other cases it is not. Positive (negative) in the colour bar indicates land elevation (ocean depth), respectively. ~~The reader will find~~For more informationve to compare each ridge shown here, see ~~with~~ the display presented in Fig. 1 and Fig. 5 for better geographic information, and their normal orientation in relation to the coordinate systems.

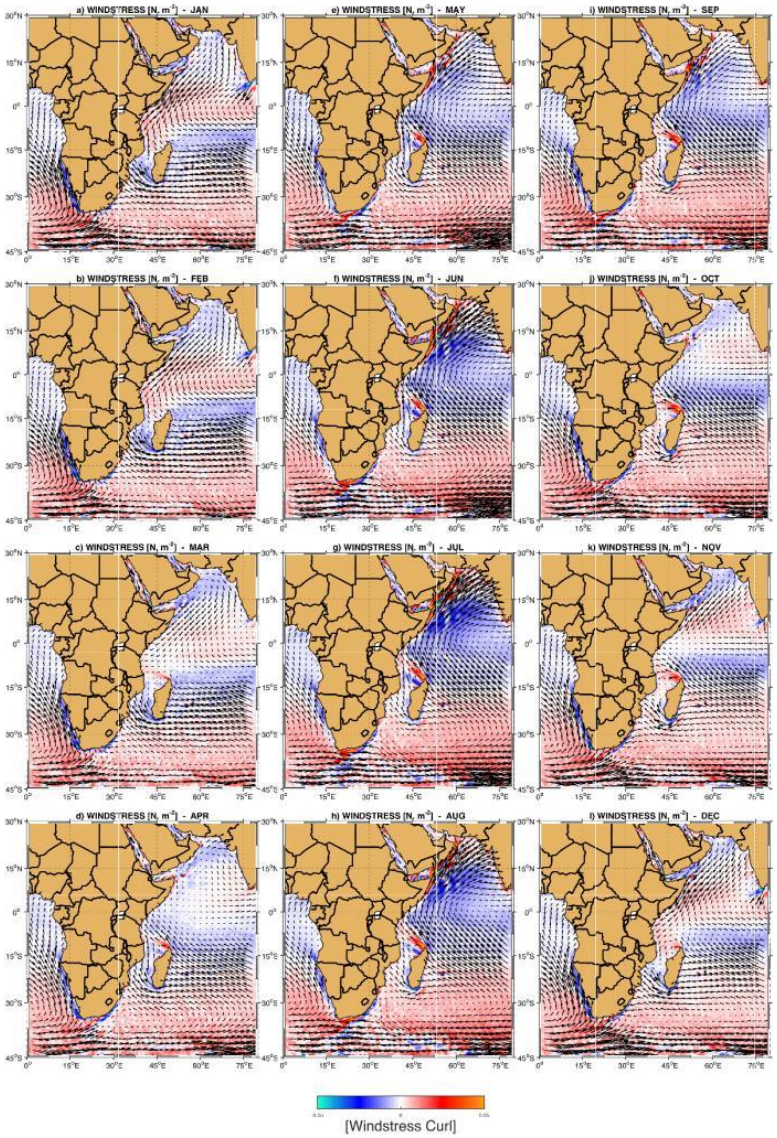

Fig. 4: Monthly climatologies (January to December) of the windstress (vectors) and winstress-curl ($\nabla \times \tau$) (colours) derived from the Scatterometer Climatology of Ocean Winds (SCOW), described by Risien and Chelton (2008). Notice the influence of the monsoons expressed through the reversal of the wind directions between January (a) and July (g). Fig. extracted from Halo and Raj (2020).

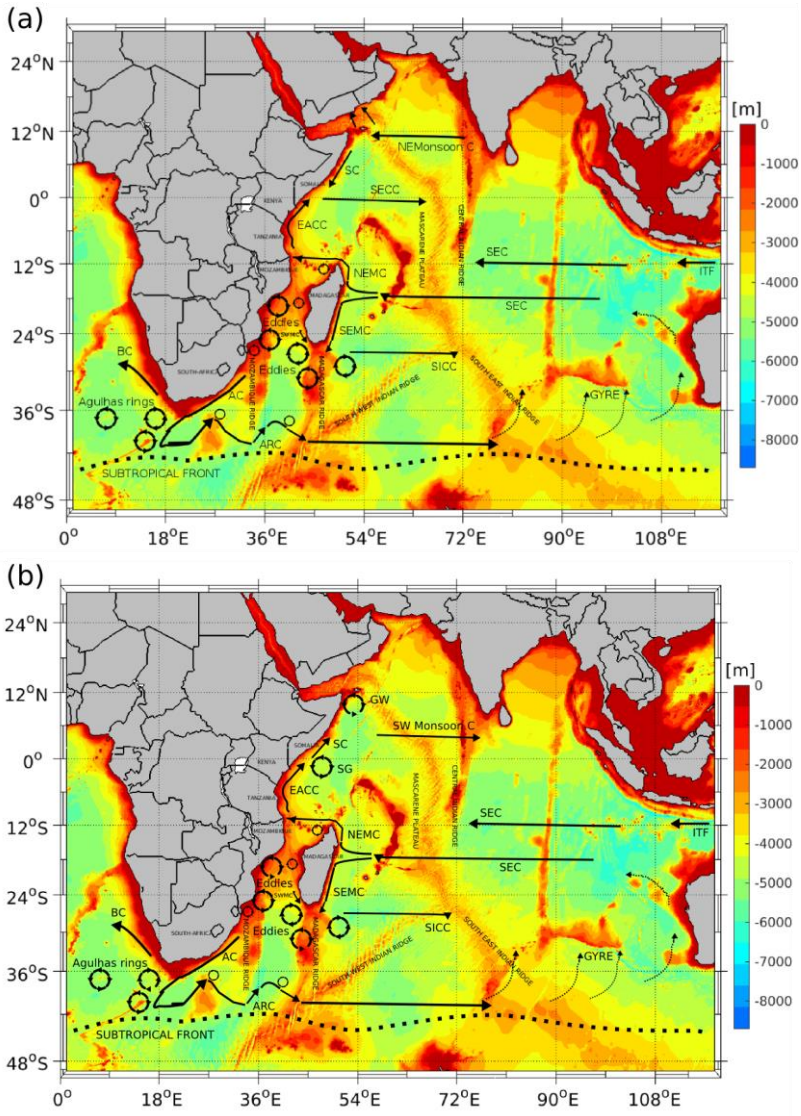

Fig. 5: Schematic of the surface currents in the Indian Ocean during different phases of the monsoonal wind~~:s~~. a) Circulation during the Southwest monsoon, and b) D~~d~~uring the n~~N~~ortheast monsoon. The background colour shows the seafloor topography, with main bathymetric features indicated by their respective labels. [Courtesy: Cedras et al., 2020; Halo and Raj (2020), adapted from Lutjeharms et al., 2006 and Schott et al., 2009]. ~~The~~ For ~~reader may find it~~ more informatiion~~ve~~ to ~~discuss~~ interpret this Fig. ~~in parallel with~~see Fig. 6~~,~~ where the intensity of the currents has been estimated with long-term oceanographic data.

Commented [MC26]: Not in the references list

Commented [MC27]: Not in the references list
Or is it just "Lutjeharms, 2006"?

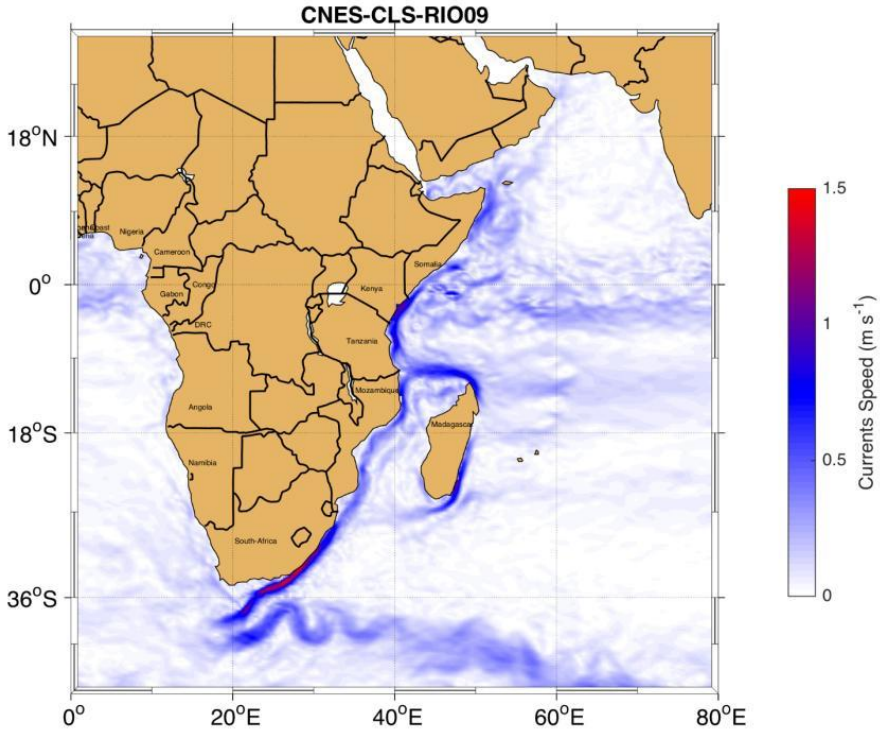

Fig. 6: Magnitude of the mean surface currents (speed in m s^{-1}) in the ~~Western Indian Ocean~~WIO, based on Mean Dynamic Topography dataset (CNES-CLS09). It reveals strong intensification of the boundary currents, with the peak in the core of the Agulhas Current on the eastern flank of the Agulhas Bank and eastern Cape province. Note the main oceanographic features of the circulation. ~~The reader may find it~~ For more information ~~ve~~ to interpret this figure, ~~discuss this Fig. with~~ see the schematic portray ~~shown~~ in Fig. 5.

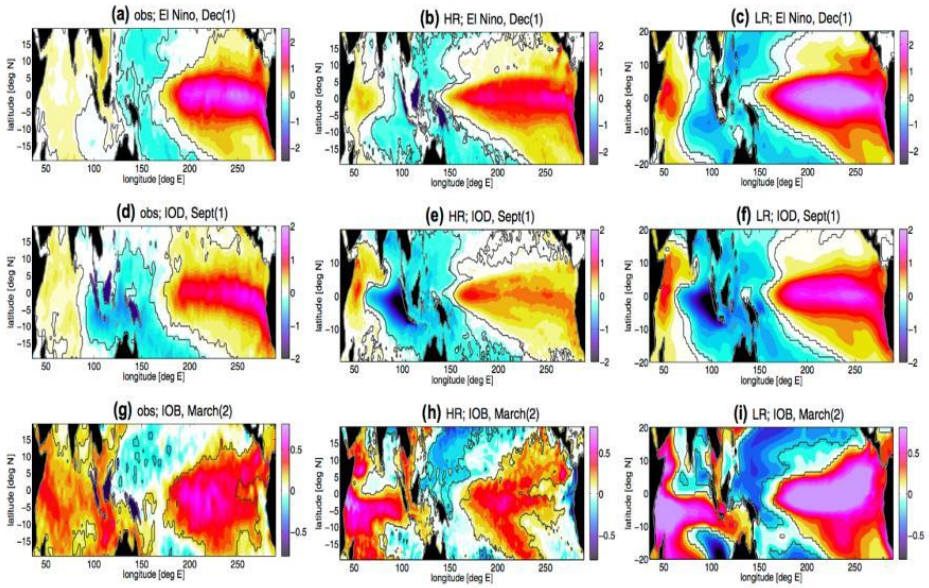

Fig. 7: Anomalies of sea surface temperature composites El Niño (a - c), Indian Ocean Dipole (d - f) and Indian Ocean Basin (g - i) in the Pacific and Indian Ocean Basin-wide. The left panels represent the phenomenon observed, and the middle panels shows their respective simulation in a numerical model at higher resolution (0.1^{o}) grid cell, and the right panels at relatively lower resolution (1^{o}) grid cell. Note that only specific months (December, September and March) have been used, representing the stronger ENSO and positive IOD phase. [Fig. extracted from Wieners et al., 2019.]

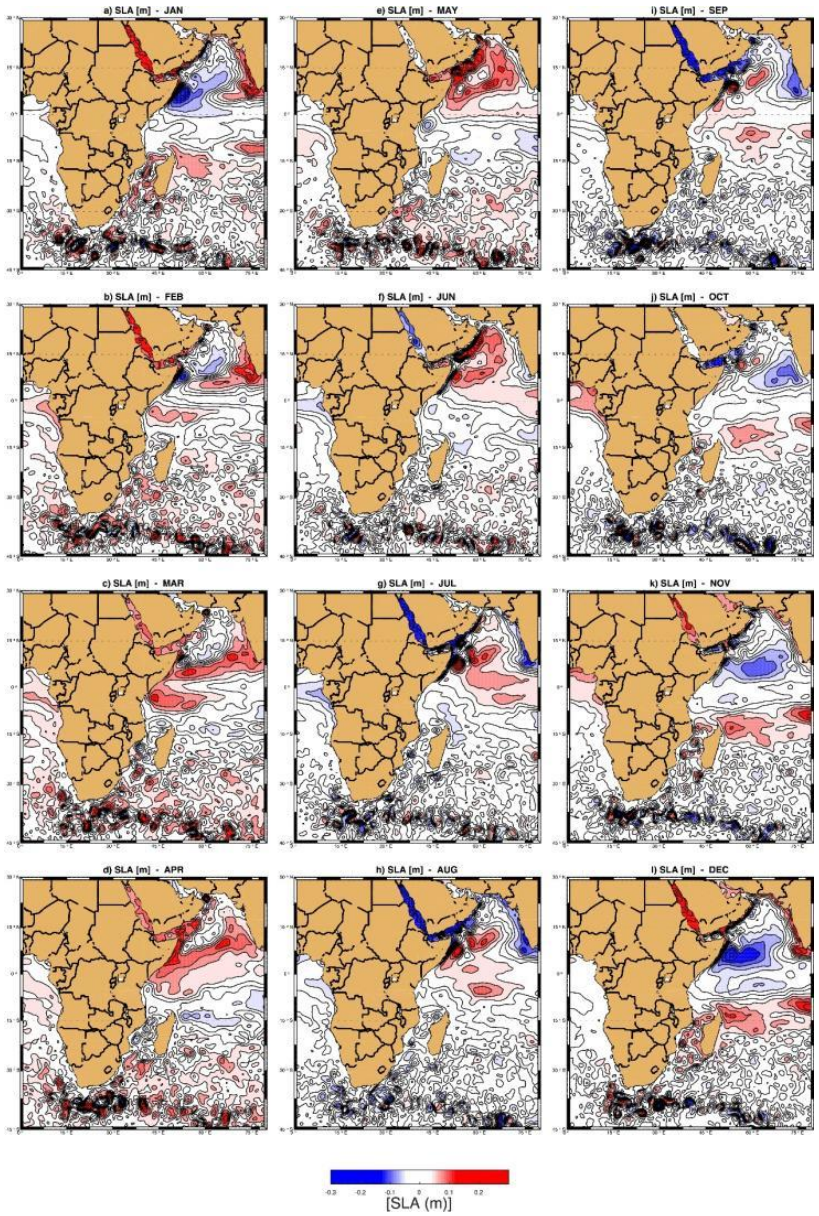

Fig. 8: Monthly mean anomalies of the sea surface height (SLA) throughout the annual cycle. It sheds on spatial and temporal levels of mesoscale variability in the ~~Western Indian Ocean~~WIO region. The dataset used is the satellite derived altimetric delayed time product for the period starting in 1993 to 2016. The dataset was downloaded from https://resources.marine.copernicus.eu/ website.

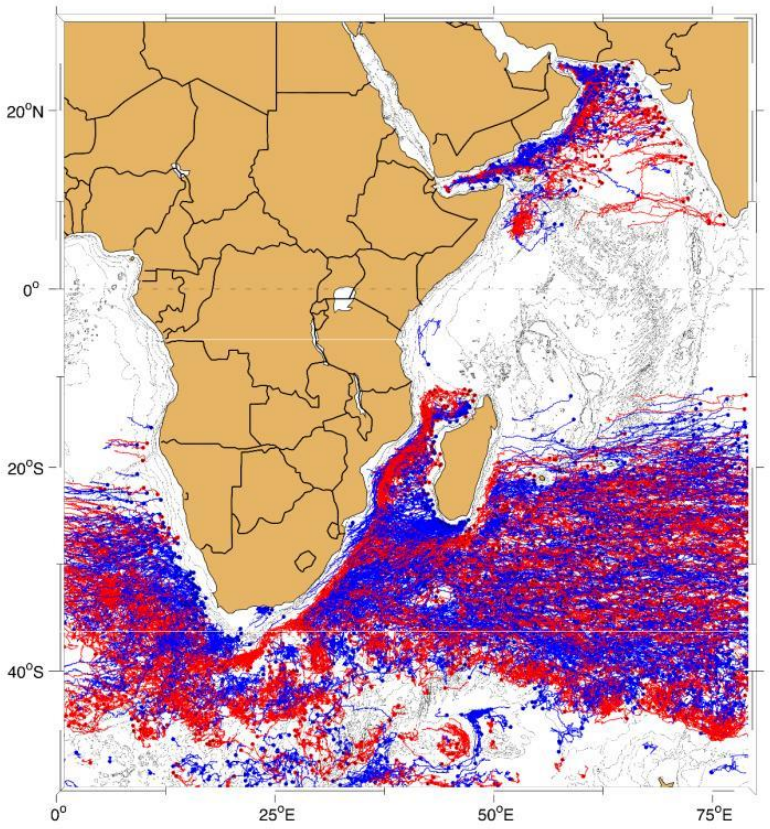

Fig. 9: Eddy generation sites, trajectories and decay. The eddies were identified using the automatic algorithm presented by Halo and Raj (2020). The dataset used is the satellite derived altimetry product absolute dynamic topography for the period starting in 1993 to 2012. The dataset was downloaded from AVISO website. Clockwise rotating eddies are shown in blue, and the anticlockwise rotating are shown in red. The background grey contours represent the seafloor topography.

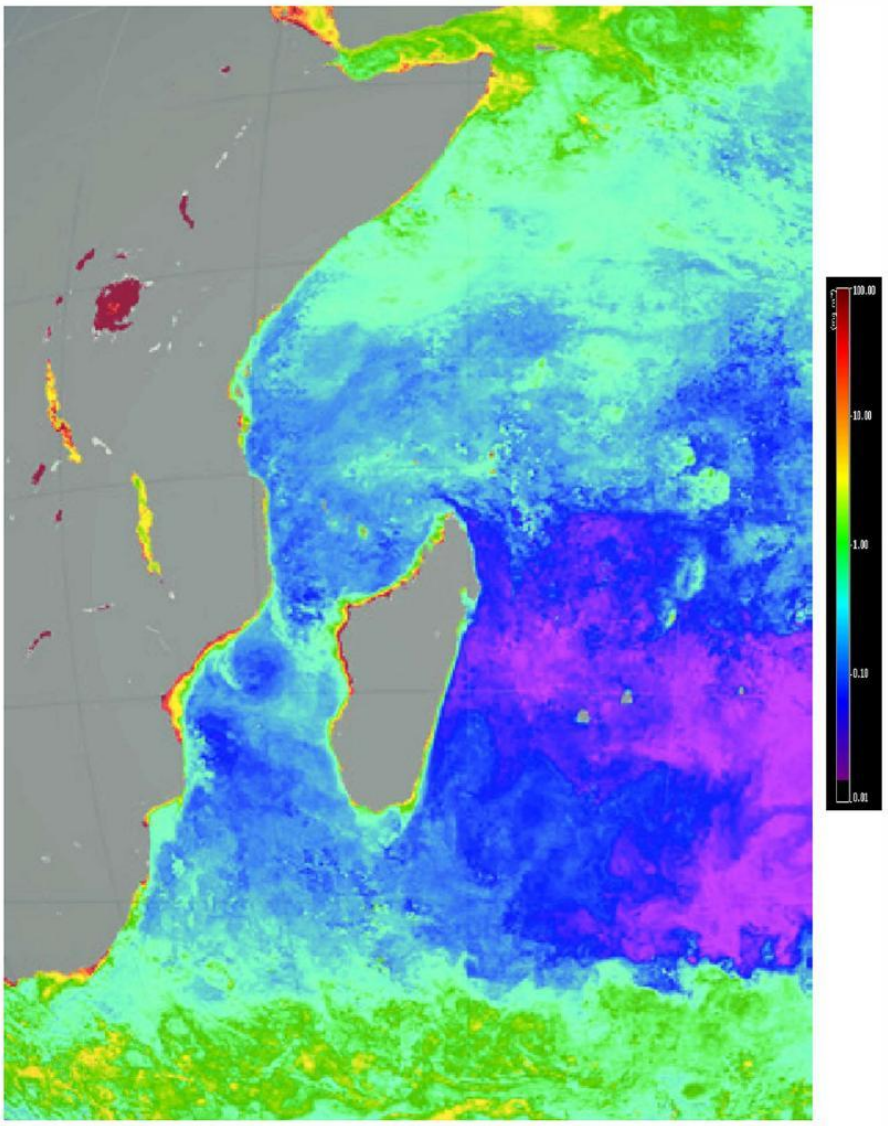

Fig. 10: Composite satellite imagery of chlorophyll concentration in the ~~Western Indian Ocean~~WIO for November 2016. Note enhanced chlorophyll concentrations mirroring main oceanographic features of the circulation, especially in the Arabian Sea, Red Sea, Somali Coast, Sofala Bank and in the Delagoa Bight off Mozambique, along the northwest and southeast coasts of Madagascar, and along the Subtropical Front. [courtesy of Huggett et al., 2017].

Commented [MC28]: Not in the references list

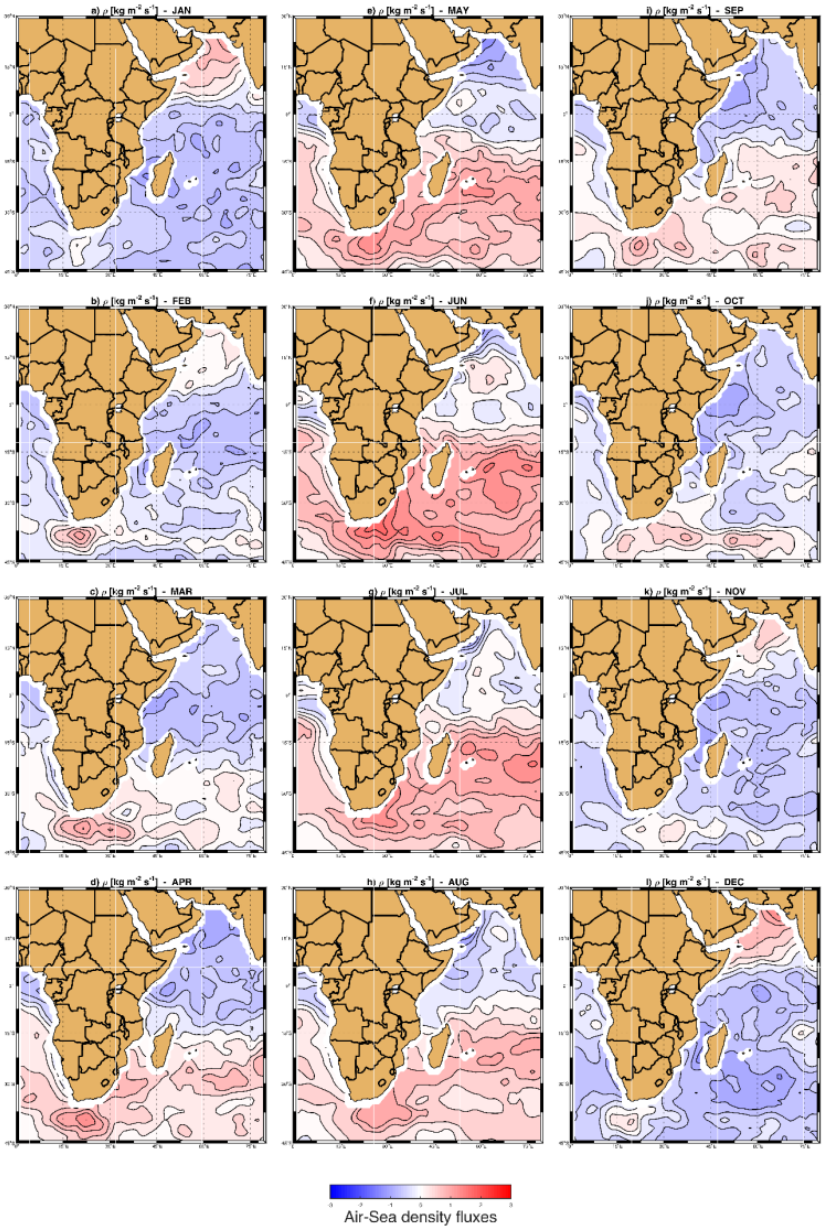

Fig. 11: Monthly mean climatology (January to December) of air-sea density fluxes (with contours of 2.5×10^{-6} kg m^{-2} s^{-1}) estimated using heat fluxes and freshwater fluxes to and from the ocean. Negative (Positive) values are indicative of density loss (gain) respectively. Density loss (gain) are indicative of oceanic heating (cooling) respectively. [Courtesy of the dataset Howe, 2008].

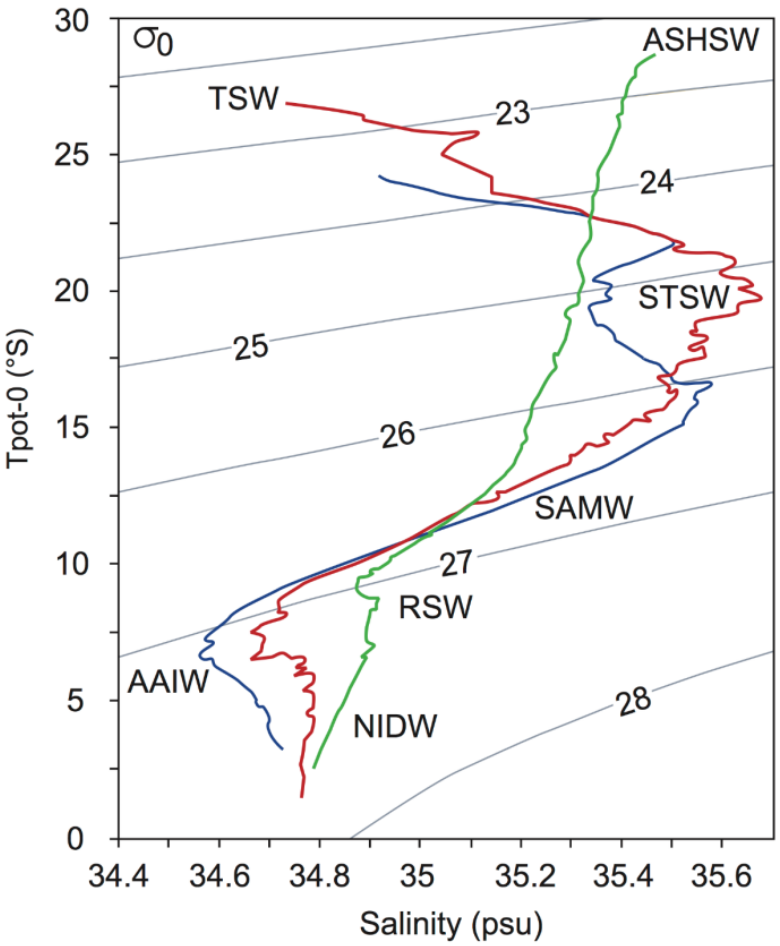

Fig. 12: Temperature/Salinity (T/S) diagram illustrating predominant water masses of the ~~Western Indian Ocean~~WIO. Antarctic Intermediate Water (AAIW), Arabian Sea water (ASHSW), Northern Indian Deep Water (NIDW), Red Sea Water (RSW), Subantarctic Mode Water (SAMW), Subtropical Surface Water (STSW), Tropical Surface Water (TSW). Adapted from Halo et al. (2017).

Commented [MC29]: Not in the references list

CASE STUDY

Commented [M30]: Where is this cited in the text?

The tropical Indian Ocean forms one of the major parts of the largest warm pool on Earth. It is not surprising that its interaction with the overlying atmosphere plays a crucial role in influencing the climate system at regional and global scales. As unprecedented, the tropical ~~western Indian Ocean~~WIO is warming at a fastest rate than any other in the world's ocean. Severe catastrophic flooding/drought events over the ~~western Indian Ocean~~WIO rim's countries are directly linked with dynamic climate modes of oceanic variability such as Indian Ocean Dipole and El-Niño Southern Oscillation (ENSO). During the worst ENSO of the century in 1997~~-~~-1998, the ENSO driven flooding/droughts ~~have been~~were reported to ~~as~~ have~~ing~~ caused thousands of deaths and misplaced hundreds of thousands of people in the WIO region. The need for better prediction of Indian Ocean climate variability is essential. Interestingly, coral records suggest a strong linkage between the ~~Western Indian Ocean~~WIO sea surface temperature and the ENSO. A case study by Zinke et al. (2008) based on analysis of coral *γ*18O*seawater* derived from both coupled ratio between chemical elements Strontium (Sr) and Calcium (Ca), i.e. Sr/Ca and salinity measurements, rainfall and rate of precipitation minus evaporation in *Porites* of Mayotte corals, in Comoros Archipelagos between 1881 and 1994 has enabled ~~to~~ reconstruction of the ~~western Indian Ocean~~WIO hydrological historical data. The results reveal that the balance between precipitation and evaporation rates varies on timescales of five to six ~~5-6~~ years and 18 - 25 years. High and low oceanic surface temperatures are found to be linked with positive and negative *γ*18O*seawater*. It also has been found that n~~N~~egative freshwater balance at Mayotte island are linked with warm ENSO events. The study highlights the importance and synergies between the physical environmental forcing on critical habitats of the WIO region on climatological timescales. It also reinforces the need for much denser network of *γ*18O*seawater* reconstruction for a better assessment of spatial patterns of hydrological conditions in the region.

Formatted: Font: Italic